Journal of Theoretical and Applied Vibration and Acoustics 9(1) 29-59 (2023)

I S A V

Journal of Theoretical and Applied

Vibration and Acoustics

journal homepage: http://tava.isav.ir

Vibrations of finite beams on nonlinear Kelvin–Voight foundations subjected to a traveling mass

Ghasem Zolfaghari[a], **Mohammad Mahdi Jalili**[*,b]

[a]*M.Sc. Student, Department of Mechanical Engineering, Yazd University, Yazd, IRAN*

[b]*Associate Professor, Department of Mechanical Engineering, Yazd University, Yazd, IRAN*

Research Article

ARTICLE INFO

Article history:
Received 6 December 2022

Received in revised form
12 March 2023

Accepted 5 May 2023

Available online 11 May 2023

Keywords:
Traveling mass

Kelvin–Voight foundation

Nonlinear vibration

Multiple scales method

Jump phenomenon

ABSTRACT

With the development of high-speed trains, the interest in studying the possibility of resonance in rail and railroad vehicles has increased. In this paper, an Euler–Bernoulli beam model rested on a nonlinear Kelvin–Voight viscoelastic foundation is used to investigate the vibration of the system due to a moving mass. The Galerkin method is used to discretize the solutions of the non-linear partial differential equations of motion to the time and position functions. The method of multiple scales is then used to obtain the frequency of the system's responses. The steady-state responses of the primary, sub, and superharmonic resonances are then obtained. The effects of different parameters, such as moving mass suspension characteristics, the foundation's nonlinearity and damping coefficients, and rail roughness on the system response, are examined. As a case study, a conventional railroad track is used for dynamic simulation, and the jump phenomenon in the response is detected for all superharmonic resonances. The results show that the backbone curve is not observed for the superharmonic resonance cases. Additionally, for the subharmonic resonance cases, the steady-state amplitude of the frequency response decreases by increasing the nonlinear stiffness coefficient.

© 2023 Iranian Society of Acoustics and Vibration, All rights reserved.

1. Introduction

Due to wide engineering applications, vibration analysis of finite beams on visco-elastic foundations has been significantly studied in recent years. Interaction between a moving vehicle and a beam resting on a visco-elastic foundation is a practical problem in many engineering applications. Determining the impact of the effects on the railway track structures, decreasing the noise and vibration in the train and railway, and increasing the ride comfort of the passengers have

[*] Corresponding author.
E-mail address: jalili@yazd.ac.ir (M.M. Jalili)

http://dx.doi.org/10.22064/tava.2024.2013047.1230

always been of interest to researchers. Vibration analyses of such coupled systems have been addressed in the literature. Some of them consider the whole train as a moving load. For example, Dong et al. [1] used a finite element model to determine the wheel and rail contact forces, in which the wagon was modeled as a moving force. In this two-dimensional model, the rail is considered an Euler-Bernoulli beam placed on the sleepers and the ballast. Pfaffinger and Dual used a similar model to investigate the rail mode shapes and frequencies [2]. Celebi [3] extracted the forces acting on the rail foundation using the finite element simulation of the rail and the rail foundation excited by the moving load. Moreover, Dimitrovova et al. [4] studied the influence of a sudden change in the rail foundation stiffness on the critical velocity of the moving load related to the Euler-Bernoulli beam and its application in high-speed trains.

In addition to the simple models presented in the above studies, there are more complete models, including the wagon body, bolster, bogie, and wagon suspension system. Zheng and Fan [5] used a simple mass, spring, and damper model for the wagon moving on the rail, considered an Euler-Bernoulli beam that rests on a viscoelastic substrate. Zhai and Sun [6] used a model that included two sub-models of railroad vehicles and the rail and its substrate to determine the vertical forces acting on the rail. In this study, the wagon is modeled as a ten Degrees of Freedom (DOF) system, and the railway is modeled as an infinite Euler-Bernoulli beam located on two layers of sleeper and ballast. Sun and Dhanasekar [7] proposed a similar model to investigate the contact forces between the wheels and the rails at the contact point caused by the wheel's damage. The 10 DOF wagon model is used in this model, which moves on the Timoshenko beam rail. Moreover, the rail is placed on a linear foundation consisting of four layers: sleeper, ballast, sub-ballast, and subgrade.

The nonlinear vibration of the beams due to stationary or moving loads has been investigated in a few recent works. Coskun and Engin [8] studied the nonlinear vibration of an elastic beam resting on a linear tensionless Winkler foundation and excited by a concentrated stationary force at its midpoint. Investigating the effect of moving load on beam vibrations is of interest to researchers due to its many applications. In some studies, the amount of this load is assumed to be constant. For example, Ansari et al. [9, 10] studied the vibration of a finite Euler–Bernoulli beam supported by a non-linear viscoelastic foundation traversed by a constant moving load. Wayou et al. [11] investigated the nonlinear dynamics of an Euler–Bernoulli beam subjected to a constant moving load, including the moving load inertia in the Duffing Equation. Due to the vibrations of the beam due to the moving load, the contact force on the beam changes. Therefore, this load is modeled as a periodic force in some research. For instance, using a two-dimensional spectral balance method to determine the solution of extended Duffing's system, Kang and Tan [12] investigated the nonlinear response of a beam subjected to quasi-periodically modulated excitations. Santee and Goncalves [13] studied the vibration of a beam on a nonlinear elastic foundation due to periodic fixed forces. Froio et al. [14] presented the numerical finite element model to analyze the vibration of a simply supported Euler-Bernoulli beam. It is supported by a spatially homogeneous nonlinear cubic elastic Winkler foundation due to a concentrated moving force. It was attempted to investigate the dependency of the critical speeds on the mean value of the harmonic force and its vibration frequency. Zhen et al. [15] investigated the steady-state responses of an infinite Euler-Bernoulli beam rested on a nonlinear foundation and subjected to a harmonic moving force.

As revealed in the literature review, in most of the research related to the nonlinear oscillations of beams resting on nonlinear foundations, the beam is excited by the moving load. When the moving

mass is high against the mass of the beam, the load inertia cannot be neglected, and the moving load assumption is inaccurate. Train–track interaction is one of the applications of such a system, in which the rail is modeled as a beam supported by a viscoelastic foundation and subjected to a traveling mass. According to the best of the authors' knowledge, analytical investigating of the vibration of beams rested on nonlinear foundations and subjected to traveling mass moving on rail irregularities has not yet been introduced in the available literature. In this paper, the response of a finite Euler-Bernoulli beam on a nonlinear Kelvin–Voight viscoelastic foundation is investigated. A parametric sensitivity analysis is done on the influences of rail irregularities and the foundation characteristics on the frequency responses. A moving railroad vehicle (moving mass) passes over a railroad track (finite beam) resting on ballast (non-linear viscoelastic foundation), which comprises the case study in this paper. The Euler–Bernoulli beam theory is employed to model the finite beam. The Galerkin method is utilized to discretize the governing equations, and the method of multiple scales (MMS) is applied to obtain the system's non-linear responses.

2. System model

The main purpose of the present research is to study the effect of different parameters of the railroad vehicle, rail, and its foundation on the frequency response (FR) of the system. The wagon model consists of the wagon body, the spring, and the damping elements representing the vehicle suspension system. In this model, the dynamic effect of the wheels is ignored, and it is assumed that the contact of the wagon mass suspension system with the rail is always established. The track submodel consists of the rail, the pads, the fasteners, the sleepers, the ballast, the sub-ballast, and the subgrade. In this paper, the rail is modeled as a continuous beam with vertical deformation, which ignores torsion along its length. Also, a non-linear Kelvin–Voight substrate model is used instead of all the foundation layers of the rail. A schematic of the model considered in this research, including railroad vehicle, rail, and its viscoelastic foundation, is shown in Figure 1. The system consists of an Euler-Bernoulli beam on a nonlinear Kelvin–Voight viscoelastic substrate oscillating under a moving mass on the rail at a constant velocity. Moreover, the suspension of the sprung mass is modeled by a linear spring (constant of k') and a linear damper (coefficient of μ').

Rail irregularities are random in nature. But in this article, these irregularities are harmonically modeled as follows:

$$I_r = \hat{a}\, sin \frac{2\pi}{\lambda} x \tag{1}$$

where, $\hat{a}$ and λ are, respectively, the amplitude and wavelength of the rail surface irregularity. If the vehicle speed ($\hat{v}$) is constant, Equation (1) can be rewritten as follows.

$$I_r = \hat{a}\, sin\, vt \tag{2}$$

where, $v = \frac{2\pi}{\lambda}\hat{v}$

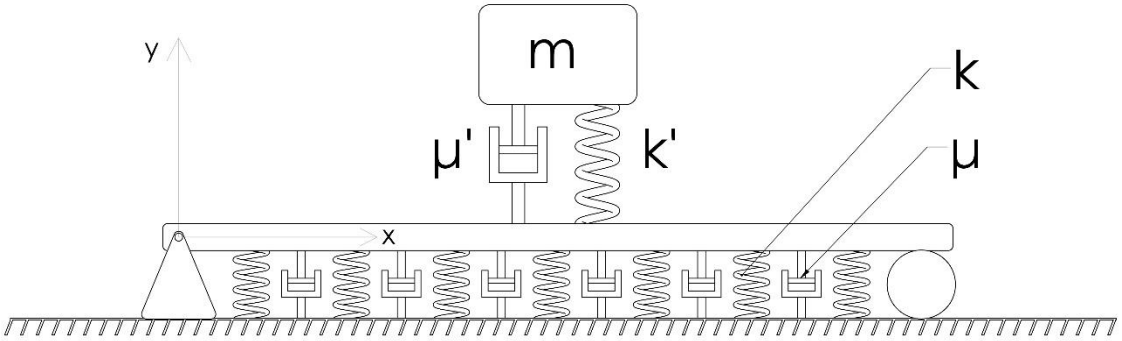

Fig. 1: Schematic of the vibration model used in this study involving the motion of a moving mass on the Euler-Bernoulli beam placed on the Kelvin-Witt nonlinear substrate

As shown in Equation (3), the Euler-Bernoulli beam theory [16] governs the vertical deflection of the rail at any point under the action of vehicle suspension and foundation forces

$$EIw_{xxxx} + kw + \alpha w^3 + \hat{\mu}w_t + \rho A w_{tt} - k'(y - w(vt,t) - \hat{a}\sin vt)\delta(x - vt) \\ - \mu'(\dot{y} - w_t(vt,t) - \hat{a}\, v\, cosvt)\delta(x - vt) = 0 \tag{3}$$

The wagon body is connected to the rail via the vehicle suspension and presents a vertical motion. As shown in Figure 1, the equation of motion of the wagon body is deduced as follows:

$$m\ddot{y} + k'(y - w(vt,t) - \hat{a}\sin vt) + \mu'(\dot{y} - w_t(vt,t) - \hat{a}\, v\, cosvt) + mg = 0 \tag{4}$$

where k, α and $\hat{\mu}$ represent the linear and non-linear stiffness coefficients and the damping coefficient of the foundation, respectively. The modulus of elasticity, the second moment of the inertia, the density, and the cross-section area of the beam are denoted as E, I, ρ, and A, respectively. Also, m and v are the mass and velocity of the moving mass, respectively, and $\hat{a}$ is the amplitude of the rail surface roughness. In addition, w and y indicate the transverse displacement of the beam and the vertical displacement of the moving mass, respectively.

The rail is assumed to be simply supported at both ends, and therefore, its boundary conditions are considered as follows:

$$w = w_{xx} = 0\ at\ \begin{cases} x = 0 \\ x = l \end{cases} \tag{5}$$

To use the Galerkin method, the transverse displacement of the beam is considered as follows:

$$w = \sum_{h=1}^{N_c} u_h(t) sin\frac{h\pi x}{l} \tag{6}$$

where, $u_h(t)$ is the h^{th} generalized coordinates of the beam vertical deflection and N_c is the number of modes considered.

Substituting Equation (6) into Equations (2) and (3) and considering $N_c = 1$ yields:

$$\begin{aligned} EI\,(\frac{\pi}{l})^4\,u(t)\,sin\frac{\pi x}{l} + k\,u(t)\,sin\frac{\pi x}{l} + \alpha u(t)^3 sin^3\frac{\pi x}{l} + \hat{\mu}\,\dot{u}(t)\,sin\frac{\pi x}{l} + \rho A\,\ddot{u}(t)\,sin\frac{\pi x}{l} \\ - k'\left(y - u(t)\,sin\frac{\pi vt}{l} - \hat{a}\,sin\,vt\right)\delta(x - vt) \\ - \mu'\left(\dot{y} - \dot{u}(t)\,sin\frac{\pi vt}{l} - \hat{a}\,v\,cosvt\right)\delta(x - vt) = 0 \end{aligned} \tag{7}$$

$$m\ddot{y} + k'\left(y - u(t)\,sin\frac{\pi vt}{l} - \hat{a}\,sin\,vt\right) + \mu'\left(\dot{y} - \dot{u}(t)\,sin\frac{\pi vt}{l} - \hat{a}\,v\,cosvt\right) + mg = 0 \tag{8}$$

where for simplification $u_1(t)$ is written as $u(t)$.

Multiplying Equation (5) by $sin\,(\pi x/l)$ and then applying integral in the beam length yields the second-order ordinary differential equations of the beam vertical vibration in terms of generalized coordinate $u(t)$ as follows:

$$\begin{aligned} \ddot{u} + \omega_1^2 u + \alpha_c u^3 + \mu_c \dot{u} - k_c'(y - u\,sin\Omega t - \hat{a}\,sin\,vt)sin\Omega t \\ - \mu_c'(\dot{y} - \dot{u}\,sin\Omega t - \hat{a}\,v\,cosvt)sin\Omega t = 0 \end{aligned} \tag{9}$$

where $\omega_1^2 = \frac{EI}{\rho A}\left[\frac{\pi}{l}\right]^4 + \frac{k}{\rho A}$, $\alpha_c = \frac{3}{4}\left[\frac{\alpha}{\rho A}\right]$, $\mu_c = \frac{\hat{\mu}}{\rho A}$, $k_c' = \frac{2k'}{\rho A l}$, $\Omega = \frac{\pi v}{l}$ and $\mu'_c = \frac{\mu'}{\rho A}$.

Also, Equation (8) can be rewritten as follows:

$$\ddot{y} + \omega_2^2(y - u\,sin\Omega t - \hat{a}\,sin\,vt) + \mu_d'(\dot{y} - \dot{u}\,sin\Omega t - \hat{a}\,v\,cosvt) + g = 0 \tag{10}$$

in which $\omega_2^2 = \frac{k'}{m}$ and $\mu'_d = \frac{\mu'}{m}$.

Preventing the resonance phenomenon in engineering problems is one of the major challenges in mechanical engineering and vibration issues. Thus, the excitation frequency of the system must be far from the resonant frequencies. In this regard, different types of resonances that can occur for the existing system are discussed.

3. Perturbation analysis of the system

3.1 Primary resonances

In this paper, the MMS is used to determine an analytical solution for the differential Equations (9) and (10). In this method, the solution can be expressed by expansions, which are functions of multiple-independent scales T_i. Correspondingly, time derivatives can be transformed into expansions in terms of the partial derivatives with respect to independent scales as:

$$\begin{aligned} \frac{d}{dt} &= D_0 + \varepsilon D_1 \\ \frac{d^2}{dt^2} &= D_0^2 + 2\varepsilon D_0 D_1 + \varepsilon^2(D_1^2 + 2D_0 D_2) \end{aligned} \tag{11}$$

in which $D_i = \frac{d}{dT_i}$, $T_i = \varepsilon^i t$ and the symbol ε is a small parameter for the time scale [17]. The expansion form of the solution of Equations (9) and (10) can be written as:

$$u = u_0 + \varepsilon u_1$$
$$y = y_0 + \varepsilon y_1 \tag{12}$$

Substituting Equations (11) and (12) into Equations (9) and (10) and equating the coefficients of ε^0 and ε^1 to zero, one acquires:

$$\begin{cases} D_0^2 u_0 + \omega_1^2\, u_0 = 0 \\ D_0^2 y_0 + \omega_2^2\, y_0 = 0 \end{cases} \tag{13}$$

ε^0:

$$\begin{cases} D_0^2 u_1 + 2D_0 D_1 u_0 + \omega_1^2\, u_1 + \hat{\alpha}_c u_0^3 + \hat{\mu}_c D_0 u_0 - \hat{k}'_c y_0 sin\Omega t \\ \quad + \hat{k}'_c\, u_0 sin^2\Omega t + \hat{k}'_c \tilde{a}\, sin\, vt\, sin\Omega t \\ \quad - \hat{\mu}'_c D_0 y_0 sin\Omega t + \hat{\mu}'_c D_0\, u_0 sin^2\Omega t + \hat{\mu}'_c \hat{a} v\, cos\, vt\, sin\Omega t = 0 \\ D_0^2 y_1 + 2D_0 D_1 y_0 + \omega_2^2 y_1 - \omega_2^2 u_0 sin\Omega t - \omega_2^2 \tilde{a}\, sin\, vt + \hat{\mu}'_c D_0 y_0 \\ \quad - \hat{\mu}'_c D_0 y_0 + \hat{\mu}'_c D_0\, u_0 sin\Omega t + \hat{\mu}'_c \hat{a} v\, cos\, vt + \hat{g} = 0 \end{cases} \tag{14}$$

in which $\alpha_c = \varepsilon\hat{\alpha}_c$, $\acute{k_c} = \varepsilon\, \hat{k}'_c$, $\mu_c = \varepsilon\hat{\mu}_c$, $\mu'_c = \varepsilon\hat{\mu}'_c$, $\mu'_d = \varepsilon\hat{\mu}'_d$, $g = \varepsilon\hat{g}$ and $\hat{a} = \varepsilon\tilde{a}$.

The solution of Equation (13) is as follows:

$$u_0 = A(T_1)e^{i\omega_1 T_0} + cc$$
$$y_0 = B(T_1)e^{i\omega_2 T_0} + cc \tag{15}$$

Inserting the solution (15) into Equation (14), the following equations are achieved:

$$\begin{aligned} D_0^2 u_1 + \omega_1^2\, u_1 = {} & -2iA'\omega_1 e^{i\omega_1 T_0} - \hat{\alpha}_c(A^3 e^{3i\omega_1 T_0} + 3A^2\bar{A}e^{i\omega_1 T_0}) - \hat{\mu}_c iA\omega_1 e^{i\omega_1 T_0} + \\ & \frac{\hat{k}'_c B}{2i}\left(e^{i(\omega_2+\Omega)T_0} - e^{i(\omega_2-\Omega)T_0}\right) + \frac{\hat{k}'_c A}{4}\left(e^{i(\omega_1+2\Omega)T_0} + e^{i(\omega_1-2\Omega)T_0} - 2e^{i\omega_1 T_0}\right) - \frac{\hat{k}'_c \tilde{a}}{4}\left(e^{i(v-\Omega)T_0} - \right. \\ & \left. e^{i(v+\Omega)T_0}\right) + \hat{\mu}'_c iB\omega_2\left(e^{i(\omega_2+\Omega)T_0} - e^{i(\omega_2-\Omega)T_0}\right) + \frac{\hat{\mu}'_c iA\omega_1}{4}\left(e^{i(\omega_1+2\Omega)T_0} - e^{i(\omega_1-2\Omega)T_0} - 2e^{i\omega_1 T_0}\right) + \\ & \frac{\hat{\mu}'_c \hat{a} vi}{4}\left(e^{i(v+\Omega)T_0} - e^{i(v-\Omega)T_0}\right) + cc \end{aligned} \tag{16}$$

$$\begin{aligned} D_0^2 y_1 + \omega_2^2 y_1 = {} & -2iB'\omega_2 e^{i\omega_2 T_0} - \frac{A\omega_2^2}{2i}\left(e^{i(\omega_1+\Omega)T_0} - e^{i(\omega_1-\Omega)T_0}\right) + \frac{\omega_2^2 \tilde{a}}{2i} e^{ivT_0} + \hat{\mu}'_d iB\omega_2 e^{i\omega_2 T_0} \\ & - \hat{\mu}'_d iA\omega_1 e^{i\omega_1 T_0} sin\Omega t - \hat{\mu}'_d \hat{a} v\, cos\, vt + cc \end{aligned} \tag{17}$$

To investigate the system resonance around the first natural frequency of the rail, the parameter Ω is considered as follows:

$$\Omega = \omega_1 + \varepsilon\sigma \tag{18}$$

Substituting Equation (18) into Equation (16) and eliminating secular terms from the resultant equations yields:

$$-2iA'\omega_1 - 3\hat{\alpha}_c A^2\bar{A} - \hat{\mu}_c iA\omega_1 - \frac{\hat{\mu}'_c iA\omega_1}{2} - \frac{\hat{k}'_c A}{2} + \frac{\hat{k}'_c \bar{A}}{4} e^{2i\varepsilon\sigma T_0} + \frac{\hat{\mu}'_c i\bar{A}\omega_1}{4} e^{2i\varepsilon\sigma T_0} = 0 \tag{19}$$

Inserting the polar form $A = \frac{1}{2}ae^{i\beta}$ into Eq. (19) and separating the real and imaginary parts of the resulting relation, the following equations are obtained:

$$\omega_1 a\left(\frac{2\sigma-\gamma'}{2}\right)-\frac{3}{4}\hat{\alpha}_c a^3-\frac{\hat{k}_c'}{4}a+\frac{\hat{k}_c'}{4}a\,cos(\gamma)+a\hat{\mu}_c'\omega_1\,sin(\gamma)=0 \tag{20}$$

$$-\omega_1 a'-\hat{\mu}_c\frac{\omega_1}{2}a-\frac{\hat{\mu}_c' A\omega_1}{2}+\frac{\hat{k}_c'}{4}a\,sin(\gamma)-a\hat{\mu}_c'\omega_1\,cos(\gamma)=0 \tag{21}$$

where $\gamma = 2\sigma T_1 - 2\beta$.

The steady-state motions correspond to $\acute{a} = \acute{\gamma} = 0$, so the FR equation is obtained as follows:

$$\left(\omega_1\sigma-\frac{3}{4}\hat{\alpha}_c a^2-\frac{\hat{k}_c'}{4}\right)^2+\frac{{\omega_1}^2}{4}(\hat{\mu}_c+\hat{\mu}_c')^2=\frac{{\hat{k}_c'}^2}{16}+(\hat{\mu}_c'\omega_1)^2 \tag{22}$$

To study the resonance of the system around the second natural frequency and state closeness of the traveling mass velocity to the second natural frequency, the detuning parameter σ is defined as follows:

$$v = \omega_2 + \varepsilon\sigma \tag{23}$$

Substituting Equation (23) into Equation (17) and eliminating secular terms from the resultant equations yields:

$$-2iB'\omega_2 e^{i\omega_2 T_0}+\hat{\mu}'_d iB\omega_2+\frac{\omega_2^2\tilde{a}}{2i}e^{i\varepsilon\sigma T_0}-\frac{\hat{\mu}_d'\hat{a}\omega_2}{2}e^{2i\varepsilon\delta T_0}=0 \tag{24}$$

Inserting the polar form $B = \frac{1}{2}be^{i\eta}$ into Equation (24), and separating the real and imaginary parts, the following equations are achieved:

$$b(\sigma-\gamma')\omega_2+\frac{\omega_2^2\tilde{a}}{2}sin(\gamma)-\frac{\omega_2\hat{a}\hat{\mu}_d'}{2}cos(\gamma)=0 \tag{25}$$

$$-\omega_2 b'-\frac{\hat{\mu}'_c b\omega_2}{2}-\frac{\omega_2^2\tilde{a}}{2}cos(\gamma)-\frac{\omega_2\hat{a}\hat{\mu}_d'}{2}sin(\gamma)=0 \tag{26}$$

where $\gamma = \sigma T_1 - \eta$.

The steady-state response is established when $\acute{b} = \acute{\gamma} = 0$, thus by applying these conditions to Equations (25) and (26) and removing γ from the resultant equations, the FR equation is obtained as follows:

$$\left(\frac{\hat{\mu}'_c b}{2}\right)^2+(b\sigma)^2=\left(\frac{\omega_2\tilde{a}}{2}\right)^2+\left(\frac{\omega_2\hat{a}\hat{\mu}_d'}{2}\right)^2 \tag{27}$$

3.2 Secondary resonances

Considering $\alpha_c = \varepsilon\hat{\alpha}_c$, $\acute{k}_c = \varepsilon\,\hat{\acute{k}}_c$, $\mu_c = \varepsilon\hat{\mu}_c$, $\mu'_c = \varepsilon\hat{\mu}'_c$, $\mu'_d = \varepsilon\hat{\mu}'_d$, and $\bar{a} = \acute{k}_c\hat{a}$, substituting Equations (11) and (12) into Equations (9)–(10) and equating the coefficients of identical powers of ε to zero, one obtains:

ε^0:

$$\begin{cases} D_0^2 u_0 + \omega_1^2\, u_0 - \bar{a}\, sin\, vt\, sin\Omega t = 0 \\ D_0^2 y_0 + \omega_2^2\, y_0 - u_0 sin\Omega t - \hat{a}\, sin\, vt = 0 \end{cases} \tag{28}$$

$$\begin{cases} D_0^2 u_1 + 2D_0 D_1 u_0 + \omega_1^2\, u_1 + \hat{\alpha}_c u_0^3 + \hat{\mu}_c D_0 u_0 - \hat{k}'_c y_0 sin\Omega t \\ +\hat{k}'_c\, u_0 sin^2\Omega t - \hat{\mu}'_c (D_0 y_0 - D_0 u_0 sin\Omega t - \hat{a} v\, cos\, vt) sin\Omega t = 0 \\ D_0^2 y_1 + 2D_0 D_1 y_0 + \omega_2^2 y_1 - \omega_2^2 u_1 sin\Omega t + \hat{\mu}'_c D_0 y_0 \\ +\hat{\mu}'_d (D_0 y_0 - D_0 u_0 sin\Omega t - \hat{a} v\, cos\, vt) + \hat{g} = 0 \end{cases} \tag{29}$$

The solution of Equation (28) can be obtained as follows:

$$u_0 = A(T_1) e^{i\omega_1 T_0} - \frac{\bar{a}}{4(\omega_1^2 - (v-\Omega)^2)} e^{i(v-\Omega)T_0} + \frac{\bar{a}}{4(\omega_1^2 - (v+\Omega)^2)} e^{i(v+\Omega)T_0} + cc \tag{30}$$

$$\begin{aligned} y_0 = B(T_1) e^{i\omega_2 T_0} & \\ & - \frac{\omega_2^2}{2i}\left[\frac{A}{(\omega_2^2 - (\omega_1+\Omega)^2)} e^{i(\omega_1+\Omega)T_0} - \frac{A}{(\omega_2^2 - (\omega_1-\Omega)^2)} e^{i(\omega_1-\Omega)T_0}\right. \\ & + \frac{P}{(\omega_2^2 - v^2)} e^{ivT_0} + \frac{P}{(\omega_2^2 - (2\Omega - v)^2)} e^{i(2\Omega - v)T_0} \\ & \left. - \frac{Q}{(\omega_2^2 - (2\Omega + v)^2)} e^{i(2\Omega+v)T_0} + \frac{Q}{(\omega_2^2 - v^2)} e^{ivT_0} - \frac{\hat{a}}{(\omega_2^2 - v^2)} e^{ivT_0}\right] + cc \end{aligned} \tag{31}$$

in which, $P = \frac{\bar{a}}{4(\omega_1^2 - (v-\Omega)^2)}$ and $Q = \frac{\bar{a}}{4(\omega_1^2 - (v+\Omega)^2)}$.

To investigate the secondary resonances, the solutions of Equations (30) and (31) should be inserted into Equation (29). The results are presented in the Appendix.

To investigate the sub-harmonic resonance case where $v + \Omega$ is close to $3\omega_1$ ($v + \Omega = 3\omega_1 + \varepsilon\sigma$), the following relation must be established to eliminate secular terms from Equation (A-1).

$$\begin{aligned} -2A' i\omega_1 - \hat{\mu}_c i\omega_1 A + 6\hat{\alpha}_c A P^2 + 6\hat{\alpha}_c A Q^2 + 3\hat{\alpha}_c \bar{A} A^2 - \frac{\hat{\acute{k}}_c\, \omega_2^2\, \lambda_1}{4} - \frac{\hat{\acute{k}}_c\, \omega_2^2\, \lambda_2}{4} - \frac{\hat{\acute{k}}_c\, A}{2} & \\ + 3Q\bar{A}^2 e^{-i\varepsilon\sigma T_0} = 0 & \end{aligned} \tag{32}$$

Inserting the polar form $A = \frac{1}{2} a e^{i\beta}$ into Equation (32) and separating the real and imaginary parts of the resulting relation, the following equations are obtained:

$$\begin{aligned} \frac{2\omega_1\sigma}{3} - \frac{2\omega_1\gamma'}{3} + 3\hat{\alpha}_c a^2 + 6\hat{\alpha}_c P^2 + 6\hat{\alpha}_c Q^2 - \frac{\hat{\acute{k}}_c\, \omega_2^2}{4(\omega_2^2 - (\omega_1+\Omega)^2)} - \frac{\hat{\acute{k}}_c\, \omega_2^2}{4(\omega_2^2 - (\omega_1-\Omega)^2)} - \frac{\hat{\acute{k}}_c}{2} & \\ + 3Qa\, cos\,(\gamma) = 0 & \end{aligned} \tag{33}$$

$$-\frac{2a'\omega_1}{a} - \hat{\mu}_c\omega_1 + 3Qa\, sin\,(\gamma) = 0 \tag{34}$$

where $\gamma = \sigma T_1 - 3\beta$.

Applying steady-state conditions $\acute{a} = \acute{\gamma} = 0$ to Eqs. (33) and (34) and removing γ from the resultant equations, the FR function is obtained as follows:

$$\left(\hat{Z} + 3\hat{\alpha}_c a^2\right)^2 + (\hat{\mu}_c \omega_1)^2 = (3Qa)^2 \tag{35}$$

where:

$$\hat{Z} = \frac{2\omega_1 \sigma}{3} + 6\hat{\alpha}_c P^2 + 6\hat{\alpha}_c Q^2 - \frac{\hat{k}_c\, \omega_2^2}{4(\omega_2^2 - (\omega_1 + \Omega)^2)} - \frac{\hat{k}_c\, \omega_2^2}{4(\omega_2^2 - (\omega_1 - \Omega)^2)} - \frac{\hat{k}_c}{2} \tag{36}$$

Similarly, for the sub-harmonic case, $v - \Omega$ is close to $3\omega_1 (v - \Omega = 3\omega_1 + \varepsilon\sigma)$ and the FR function can be obtained as follows:

$$\left(\hat{Z} + 3\hat{\alpha}_c a^2\right)^2 + (\hat{\mu}_c \omega_1)^2 = (3Pa)^2 \tag{37}$$

where:

$$\hat{Z} = \frac{2\omega_1 \sigma}{3} + 6\hat{\alpha}_c P^2 + 6\hat{\alpha}_c Q^2 - \frac{\hat{k}_c\, \omega_2^2}{4(\omega_2^2 - (\omega_1 + \Omega)^2)} - \frac{\hat{k}_c\, \omega_2^2}{4(\omega_2^2 - (\omega_1 - \Omega)^2)} - \frac{\hat{k}_c}{2} \tag{38}$$

To investigate the case of superharmonic resonance and state closeness of $(v + \Omega)$ to $\frac{1}{3}\omega_1$, the detuning parameter σ is defined as follows:

$$3(v + \Omega) = \omega_1 + \varepsilon\sigma \tag{39}$$

Substituting Equation (39) into Eq. (A-1), and eliminating secular terms from the resulting equations obtain:

$$-\frac{\widehat{k\prime}_c \omega_1^2 A}{4\left(\omega_2^2 - (\omega_1 + \Omega)^2\right)} - \frac{\widehat{k\prime}_c \omega_2^2 A}{4\left(\omega_1^2 - (\omega_1 - \Omega)^2\right)} - \frac{\hat{k}_c A}{2} + \hat{a}_1 Q^3 e^{iE\sigma T_0} = 0 \tag{40}$$

Putting polar form $A = \frac{1}{2}\alpha e^{i\beta}$ in Equation (40), and separating the real and imaginary parts, it can be shown that:

$$2\omega_1 \sigma + 6P^2 \hat{\alpha}_c + 6Q^2 \hat{\alpha}_c + 3a^2 \hat{\alpha}_c - \frac{\hat{k}_c \omega_2^2}{4\left(\omega_2^2 - (\omega_1 + \Omega)^2\right)} - \frac{\hat{k}_c \omega_2^2}{4\left(\omega_1^2 - (\omega_1 - \Omega)^2\right)} - \frac{\hat{k}_c}{2} + \hat{a}_c \frac{Q^3}{a} cos\gamma = 0 \tag{41}$$

$$-\omega_1 \hat{\mu}_c + \hat{a}_c \frac{Q^3}{a} sin\gamma = 0 \tag{42}$$

in which $\gamma = \sigma T_1 - \beta$.

Removing the variable γ from the Equations (41) and (42), the FR function can be obtained as follows:

$$[Z + 2\omega_1\sigma]^2 + [\omega_1\hat{\mu}_c]^2 = \left[\frac{\hat{\alpha}_c Q^3}{a}\right]^2 \tag{43}$$

where

$$Z = 3a^2\hat{\alpha}_c + 6P^2\hat{\alpha}_c + 6Q^2\hat{\alpha}_c - \frac{\hat{k}_c\omega_2^2}{4(\omega_1^2 - (\omega_1 + \Omega)^2)} - \frac{\hat{k}_c\omega_2^2}{4(\omega_2^2 - (\omega_1 - \Omega)^2)} - \frac{\hat{k}_c}{2} \tag{44}$$

Similarly, for the superharmonic resonance case $(v - \Omega) \approx \frac{1}{3}\omega_1$, the FR function can be obtained as follows:

$$[Z + 2\omega_1\sigma]^2 + [\omega_1\hat{\mu}_c]^2 = \left[\frac{\hat{\alpha}_c P^3}{a}\right]^2 \tag{45}$$

in which

$$Z = 3a^2\hat{\alpha}_c + 6P^2\hat{\alpha}_c + 6Q^2\hat{\alpha}_c - \frac{\hat{k}_c\omega_2^2}{4(\omega_1^2 - (\omega_1 + \Omega)^2)} - \frac{\hat{k}_c\omega_2^2}{4(\omega_2^2 - (\omega_1 - \Omega)^2)} - \frac{\hat{k}_c}{2} \tag{46}$$

4. Results and discussion

In this section, after validating the presented model to ensure the accuracy of the results, the effects of different parameters on FR of the railroad vehicle, rail, and its foundation system are numerically studied. The specifications of the railway track, its non-linear foundation, and the data for the passing train are listed in Table 1 [7, 18]. The vibration analysis of the system due to rail irregularities is considered in this section. The FR of the system is investigated for different resonance conditions.

Table 1. Characteristics of the system model [7, 18].

Symbol	Unit	Value	Symbol	Unit	Value
m	(kg)	1×10^4	E	(GPa)	200
k'	(N/m)	3×10^7	I	(m^4)	2.35×10^{-5}
α	(N/m^3)	1×10^4	A	(m^2)	7.17×10^{-3}
μ	(Ns/m)	20×10^3	k	(N/m)	1×10^{10}
μ'	(N/m^3)	1×10^4	$\hat{a}$	(m)	0.1
ρ	(kg/m^3)	7800	v	(m/s)	55

4.1 Validation

The time response of the solution method presented in this paper is validated by comparing it with the response obtained by the fifth-order Runge-Kutta numerical method. For this reason, characteristics of the system are selected from Table 1 and $\hat{a}$ and Ω are considered 1.25×10^{-2} m

and 8.5 Hz, respectively. The results are shown in Figure 2. Good agreement can be found between the response obtained by the MMS method and the results of the Runge-Kutta numerical method.

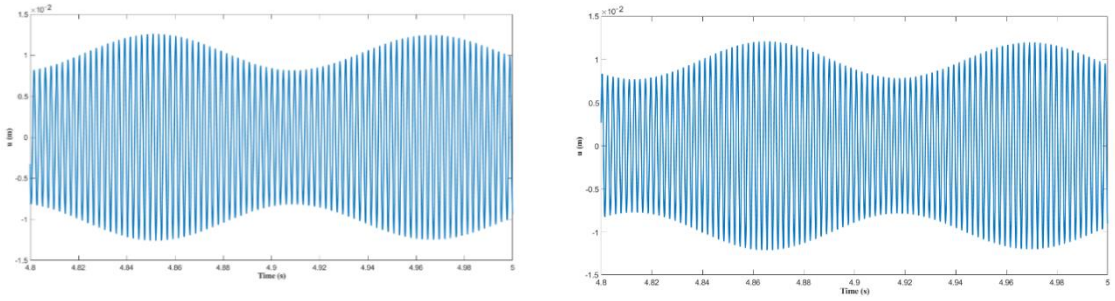

(a) **(b)**

Fig. 2: Comparison of the time response obtained by a) the MMS method with the results of b) the Runge-Kutta numerical method

4.1 Case (a) when $\boldsymbol{\Omega \approx \omega_1}$

FR curves of the system in the primary resonance cases $\Omega \approx \omega_1$ for different stiffness coefficients of the moving mass suspension are illustrated in Figure 3-a. As shown in this graph, a jump phenomenon arises, and the jump frequency and the maximum value of the FR increase with the increasing suspension stiffness.

Effects of the damping coefficient of the moving mass suspension on the FR are shown in Figure 3-b. It can be seen that the jump frequency and the maximum value of the FR would again increase with an increase in the suspension damping. Additionally, a backbone curve is observed for different jump frequencies.

Effects of linear and nonlinear stiffness and damping coefficients of the foundation on the FR are shown in Figures 3 (c-d), respectively. As shown in Figure 3-d, the jump frequency decreases with the decrease in the foundation nonlinearity. A backbone curve is not observed in this case. In other words, the nonlinear stiffness of the foundation delays the jump phenomenon but does not influence the maximum value of the FR. It can be observed from Figure 3-e that the jump frequency and the maximum value of the FR increase with the decrease in the foundation damping.

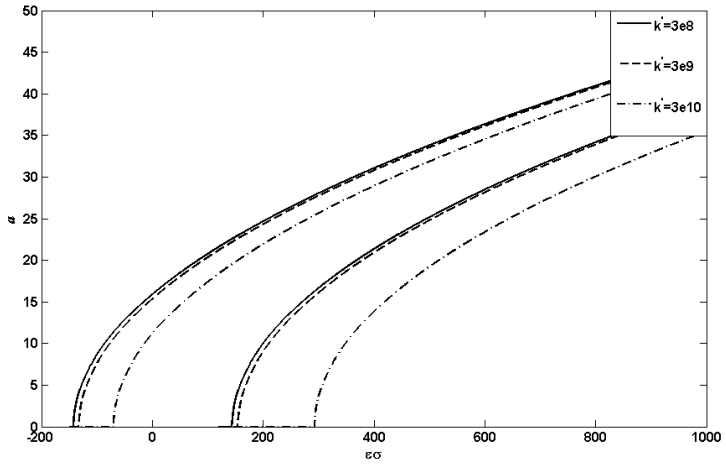

(a)

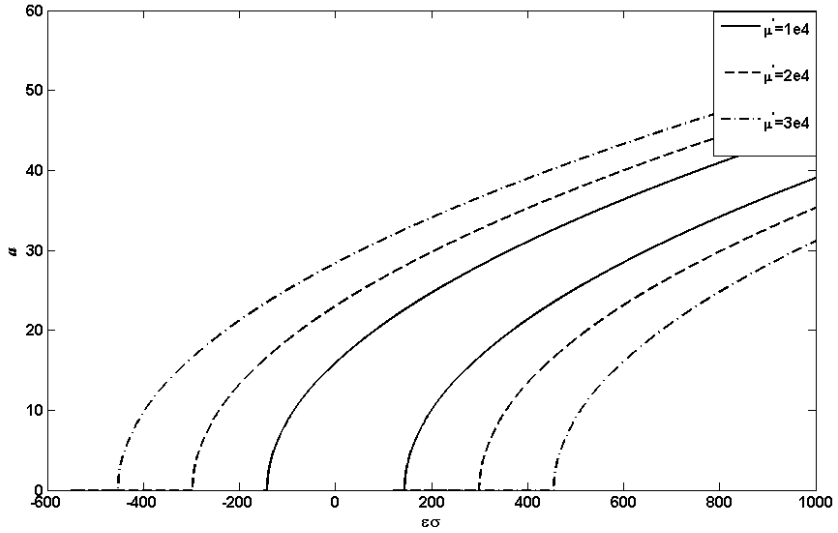

(b)

Fig. 3: Effects of a) stiffness coefficient of the moving mass suspension, b) damping coefficient of the moving mass suspension, c) linear stiffness coefficient of the foundation, d) nonlinear stiffness coefficient of the foundation, e) damping coefficient of the foundation on the FR of the rail vibration for $\boldsymbol{\Omega \approx \omega_1}$

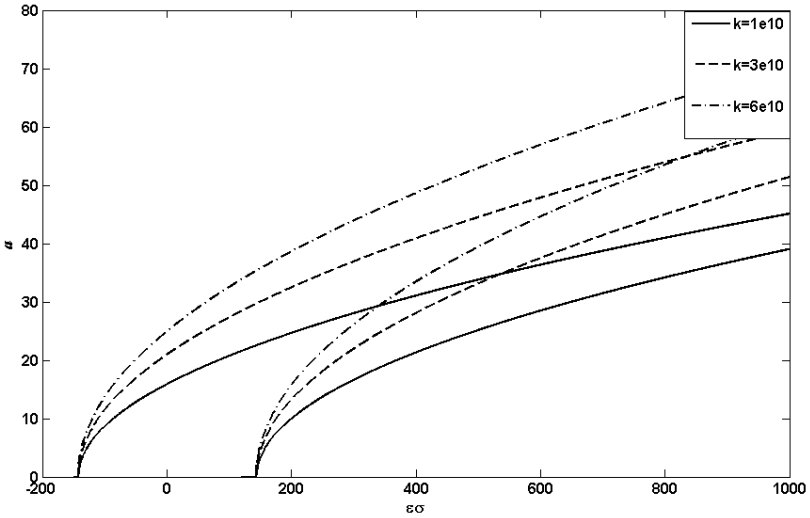

(c)

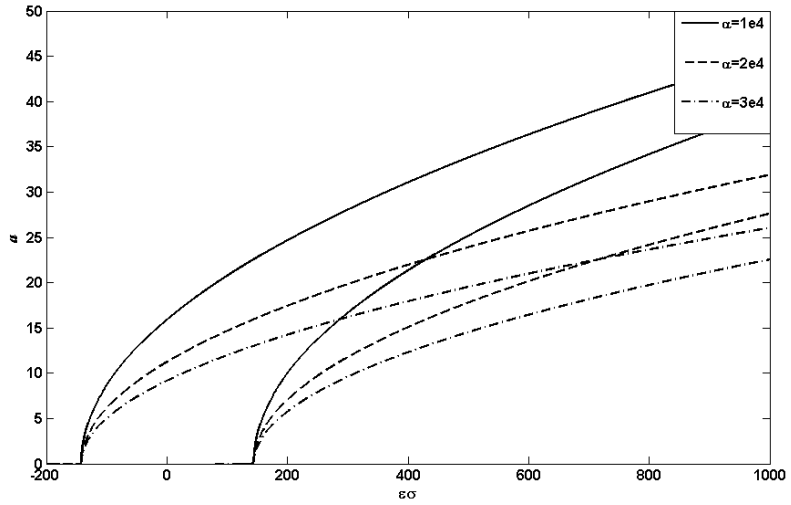

(d)

Fig. 3 (Cont.): Effects of a) stiffness coefficient of the moving mass suspension, b) damping coefficient of the moving mass suspension, c) linear stiffness coefficient of the foundation, d) nonlinear stiffness coefficient of the foundation, e) damping coefficient of the foundation on the FR of the rail vibration for $\boldsymbol{\Omega \approx \omega_1}$

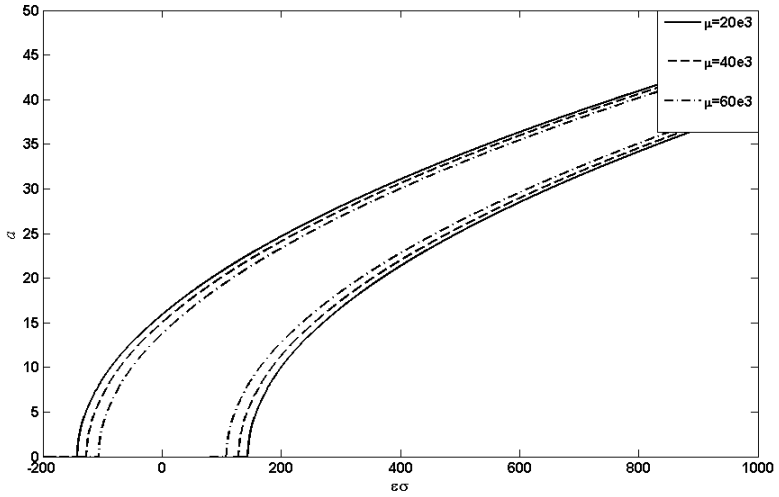

(e)

Fig. 3 (Cont.): Effects of a) stiffness coefficient of the moving mass suspension, b) damping coefficient of the moving mass suspension, c) linear stiffness coefficient of the foundation, d) nonlinear stiffness coefficient of the foundation, e) damping coefficient of the foundation on the FR of the rail vibration for $\boldsymbol{\Omega \approx \omega_1}$

4.2 Case (b) when $\boldsymbol{v \approx \omega_2}$

For this case, the variations of parameter b with $\varepsilon\sigma$, for three different values of the stiffness coefficient of the moving mass when $v \approx \omega_2$, are shown in Figure 4-a.

As shown in Figure 4-a, by increasing the moving mass's stiffness coefficient, the vehicle's steady-state amplitude increases. Moreover, in this case, the jump phenomenon does not occur in the system. Furthermore, the influence of the damping coefficient of the traveling mass on the FR of the vehicle is shown in Figure 4-b. It is evident that the amplitude of the steady-state oscillations of the vehicle decreases by increasing the damping coefficient of the moving mass.

The effects of rail vehicle mass on the FR of the system are examined, and the results are shown in Figure 4-c. As shown in this figure, as the mass of the rail vehicle increases, the amplitude of the oscillations of the moving mass around the natural frequency increases. However, by moving away from the natural frequency ω_2, increasing the mass caused a reduction in the amplitude of the vehicle oscillations.

Figure 4-d shows the effect of the rail irregularities on the FR of the system. The results show that with increasing the amplitude of rail surface roughness, the amplitude of the steady-state oscillations of the vehicle increases. This result can also be deduced from Equation (27). In addition, the amplitude of the rail roughness has a much greater effect on the FR of the system than the previous parameters. As shown in Figure 4, the jump phenomenon doesn't occur for this primary resonance case.

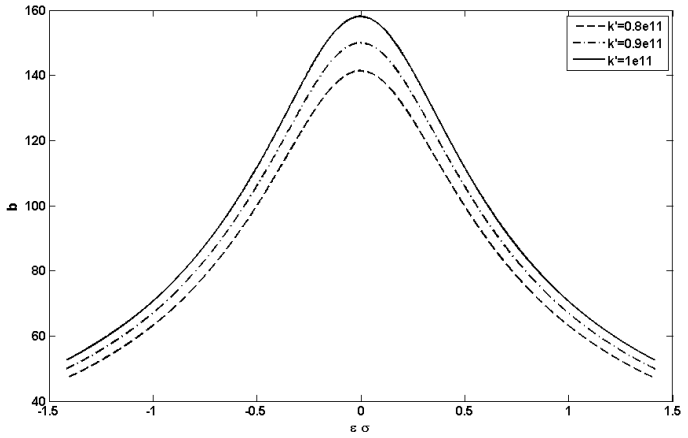

(a)

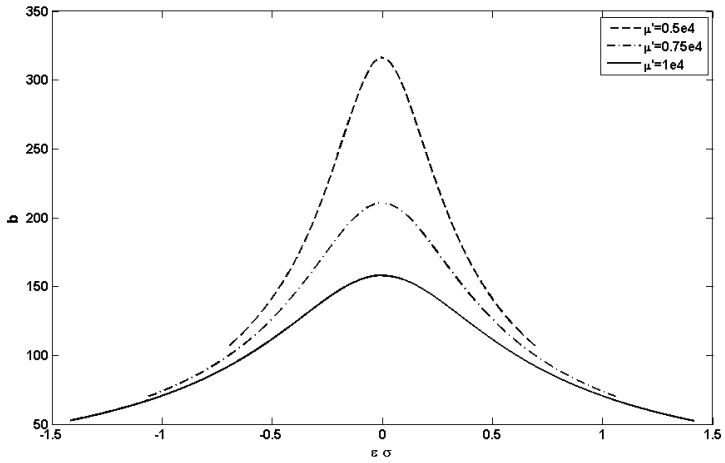

(b)

Fig. 4: Effects of a) stiffness coefficient of the moving mass suspension, b) damping coefficient of the moving mass suspension, c) vehicle mass, d) rail surface roughness on the FR of the vehicle for $\boldsymbol{\Omega \approx \omega_1}$

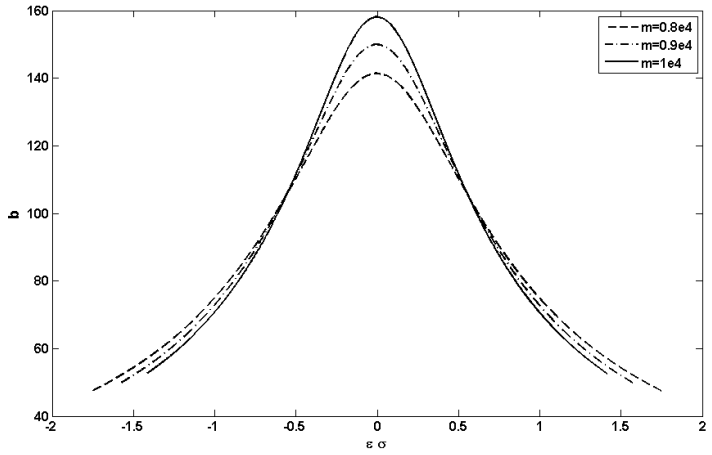

(c)

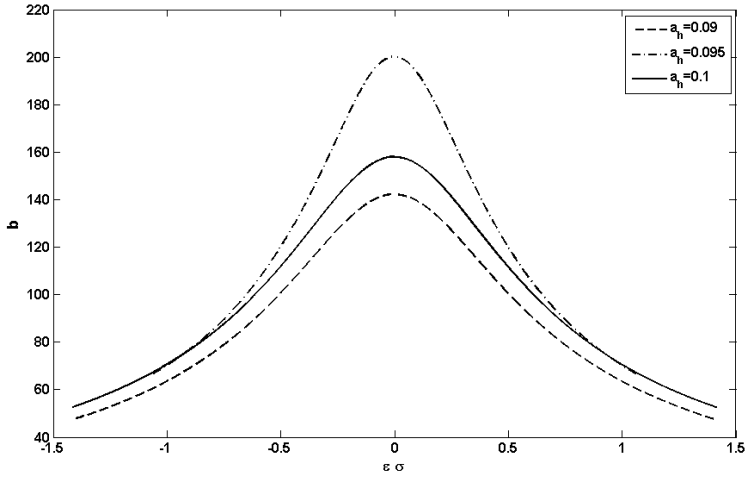

(d)

Fig. 4 (Cont.): Effects of a) stiffness coefficient of the moving mass suspension, b) damping coefficient of the moving mass suspension, c) vehicle mass, d) rail surface roughness on the FR of the vehicle for $\boldsymbol{\Omega \approx \omega_1}$

4.3 Case (c) when $\boldsymbol{v + \Omega \approx 3\omega_1}$

For this case, the influences of the linear and nonlinear stiffness coefficient and the damping coefficient of the rail foundation on the FR curves are illustrated in Figures 5(a-c), respectively. As shown in Figure 5-a, increasing the coefficient of linear stiffness of the foundation increases the amplitude of vibrations with an increase in the steady state amplitude of the rail about this subharmonic resonance.

The influence of the nonlinear stiffness coefficient of the rail foundation on the FR of the system for this subharmonic resonance case is presented in Figure 5-b. According to this figure, by decreasing the nonlinear stiffness coefficient, the steady-state amplitude of the FR increases.

Additionally, the effect of the foundation damping coefficient on the steady-state amplitude of vibration of the rail is shown in Figure 5-c. As shown in this figure, the steady-state amplitude of the rail oscillations increases with the damping coefficient of the foundation increasing.

Figure 5-d indicates the influence of the traveling mass suspension stiffness on the vibration response of the rail. It is evident that the steady-state amplitude of the FR decreases by increasing the suspension coefficient of the vehicle.

Furthermore, the influence of the suspension damping coefficient of the traveling mass on the FR of the rail is studied, and the results are presented in Figure 5-e. According to this figure, as the damping coefficient increases, the FR amplitude increases.

The effect of rail surface roughness on the FR of the system is shown in Figure 5-f. The results show that the amplitude of the steady-state response of the rail decreases by increasing the amplitude of the rail surface roughness.

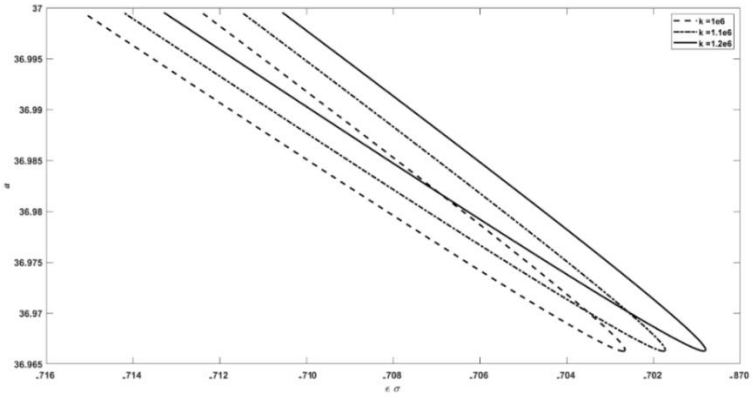

(a)

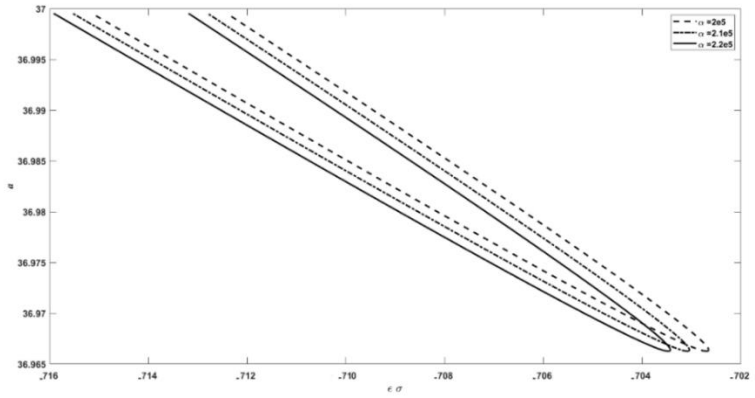

(b)

Fig. 5: Effects of a) linear stiffness coefficient of the rail foundation, b) nonlinear stiffness coefficient of the rail foundation, c) damping coefficient of the rail foundation, d) suspension stiffness coefficient of the moving mass, e) suspension damping coefficient of the moving mass, f) rail roughness on the FR of the rail vibration for $\boldsymbol{\nu + \Omega \approx 3\omega_1}$

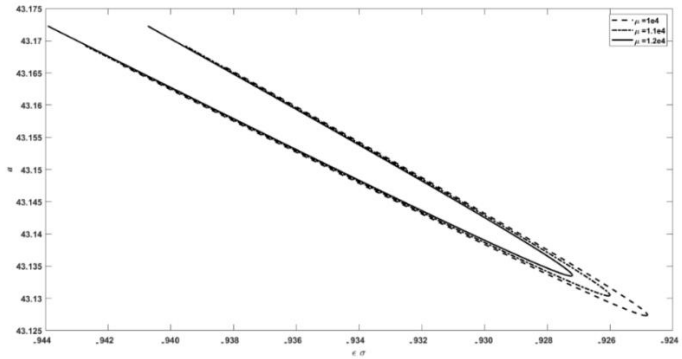

(c)

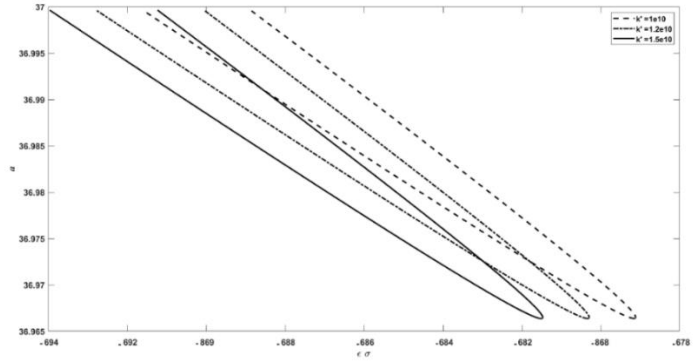

(d)

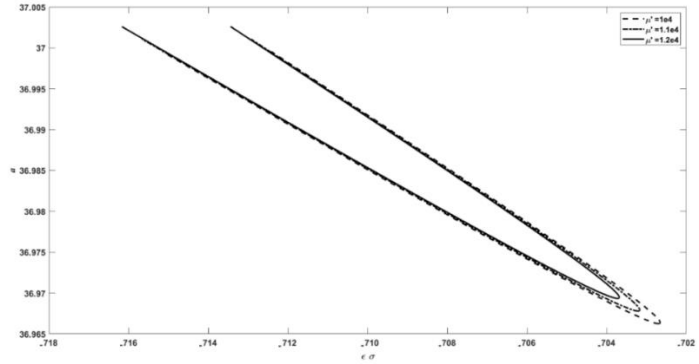

(e)

Fig. 5 (Cont.): Effects of a) linear stiffness coefficient of the rail foundation, b) nonlinear stiffness coefficient of the rail foundation, c) damping coefficient of the rail foundation, d) suspension stiffness coefficient of the moving mass, e) suspension damping coefficient of the moving mass, f) rail roughness on the FR of the rail vibration for $v + \Omega \approx 3\omega_1$

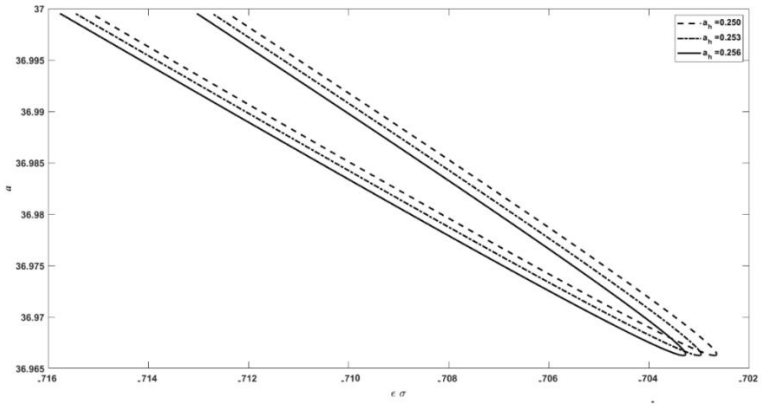

(f)

Fig. 5 (Cont.): Effects of a) linear stiffness coefficient of the rail foundation, b) nonlinear stiffness coefficient of the rail foundation, c) damping coefficient of the rail foundation, d) suspension stiffness coefficient of the moving mass, e) suspension damping coefficient of the moving mass, f) rail roughness on the FR of the rail vibration for $\boldsymbol{v + \Omega \approx 3\omega_1}$

4.4 Case (d) when $\boldsymbol{v - \Omega \approx 3\omega_1}$

For this subharmonic resonance case, the effects of different parameters on the FR of the rail are investigated and presented in Figure 6. These parameters include linear and nonlinear stiffness coefficients of the rail foundation, damping coefficient of the rail foundation, stiffness and damping coefficients of the suspension of the moving mass, and rail roughness

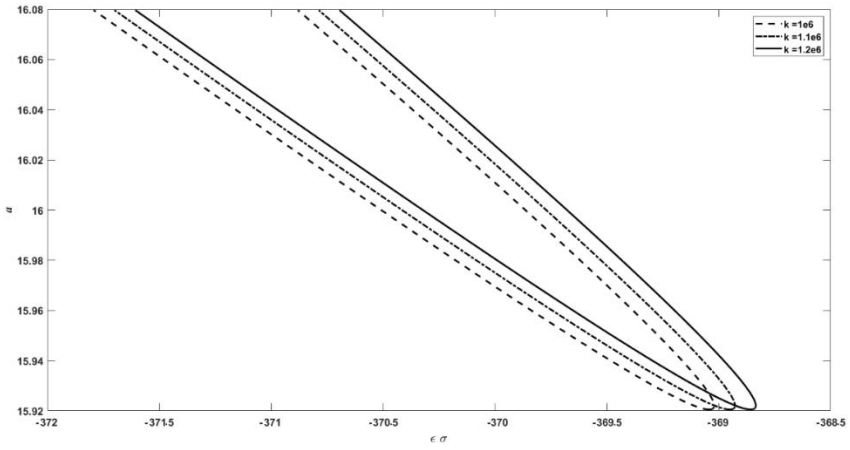

(a)

Fig. 6: Effects of a) linear stiffness coefficient of the rail foundation, b) nonlinear stiffness coefficient of the rail foundation, c) damping coefficient of the rail foundation, d) suspension stiffness coefficient of the moving mass, e) suspension damping coefficient of the moving mass, f) rail roughness on the FR of the rail vibration for $\boldsymbol{v - \Omega \approx 3\omega_1}$

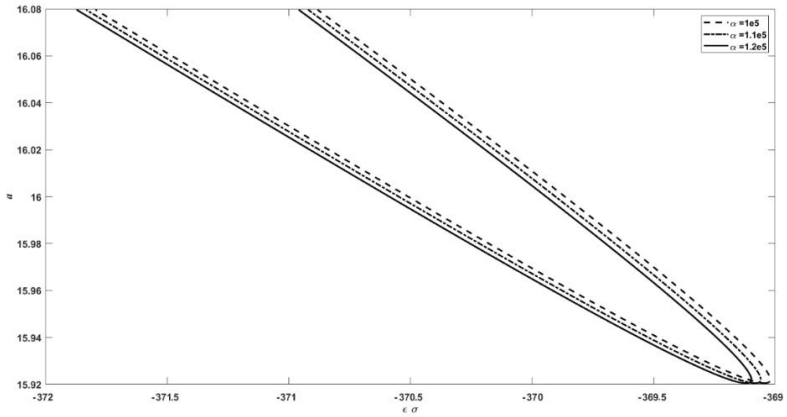

(b)

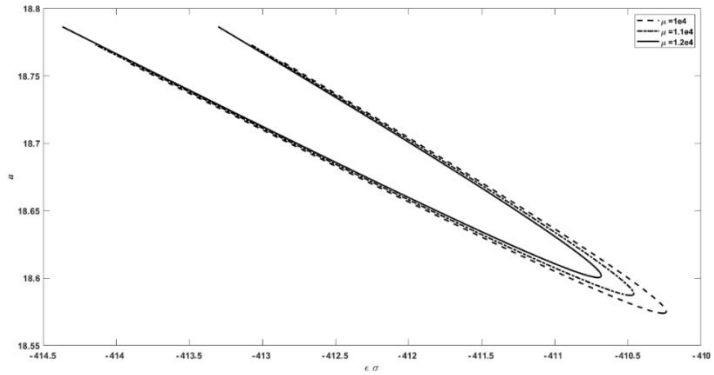

(c)

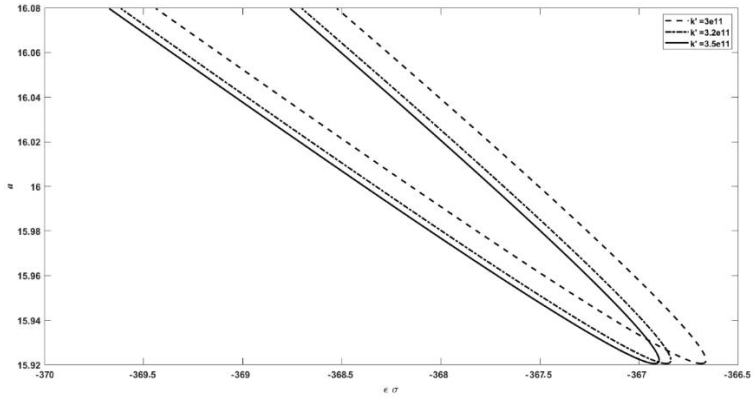

(d)

Fig. 6 (Cont.): Effects of a) linear stiffness coefficient of the rail foundation, b) nonlinear stiffness coefficient of the rail foundation, c) damping coefficient of the rail foundation, d) suspension stiffness coefficient of the moving mass, e) suspension damping coefficient of the moving mass, f) rail roughness on the FR of the rail vibration for $\boldsymbol{\nu - \Omega \approx 3\omega_1}$

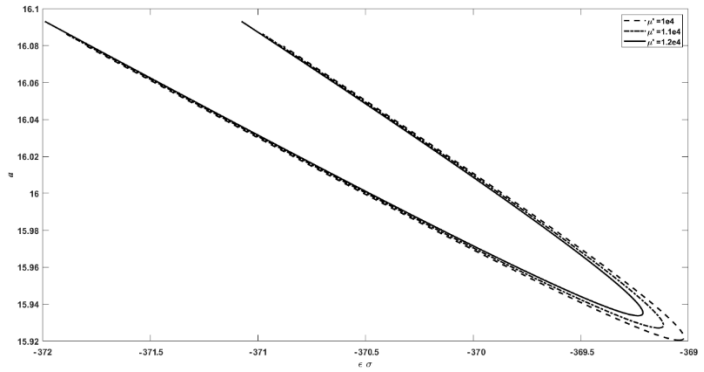

(e)

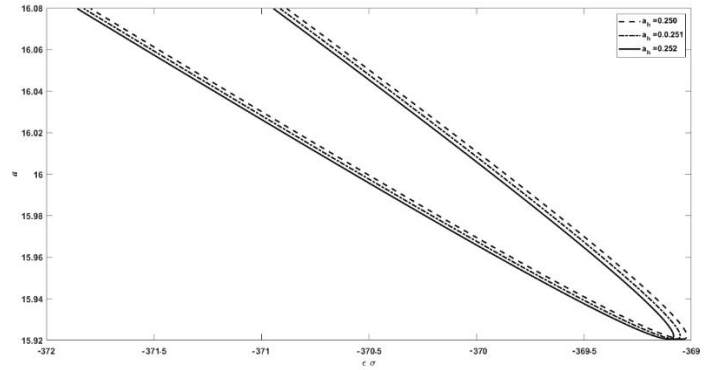

(f)

Fig. 6 (Cont.): Effects of a) linear stiffness coefficient of the rail foundation, b) nonlinear stiffness coefficient of the rail foundation, c) damping coefficient of the rail foundation, d) suspension stiffness coefficient of the moving mass, e) suspension damping coefficient of the moving mass, f) rail roughness on the FR of the rail vibration for $\boldsymbol{v - \Omega \approx 3\omega_1}$

As shown in Figure 6, with an increase in linear stiffness and damping of the rail foundation and suspension damping coefficient of the moving mass, the steady-state amplitude of the rail oscillation increases. In addition, the vibration amplitude of the rail decreases when the nonlinear stiffness of the rail foundation, the suspension stiffness coefficient of the moving mass, and the rail roughness increase.

4.5 Case (e) when $\boldsymbol{v + \Omega \approx {\omega_1}/{3}}$

The influence of the linear and nonlinear stiffness coefficients of the rail foundation, damping coefficient of the rail foundation, stiffness and damping coefficients of the suspension of the traveling mass, and rail roughness on the frequency responses of the rail for superharmonic resonance case $v + \Omega \approx {\omega_1}/{3}$, are shown in Figure 7. As shown in these graphs, the jump frequency decreases with the increase of the nonlinear stiffness coefficients of the rail foundation, stiffness coefficients of the moving mass suspension, and rail roughness. Furthermore, the jump frequency decreases with the decrease of linear stiffness coefficients of the rail foundation. The

damping coefficients of the rail foundation and the traveling mass suspension do not significantly affect the jump frequency. However, the peak value of the FR remains constant, and a backbone curve is not observed in all cases. In other words, the nonlinear stiffness of the foundation delays the jump phenomenon and does not affect the maximum value of the steady-state amplitude of the responses. As seen in Figure 7, the resonant frequency of the system occurs at a higher frequency when the velocity of the moving mass increases than when the velocity of the moving mass decreases. This is due to the bending of the FR curve to the left.

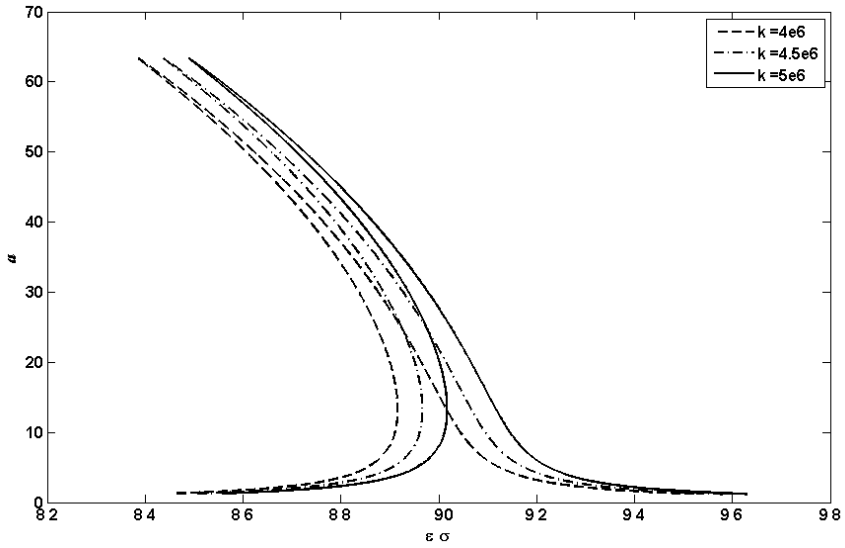

(a)

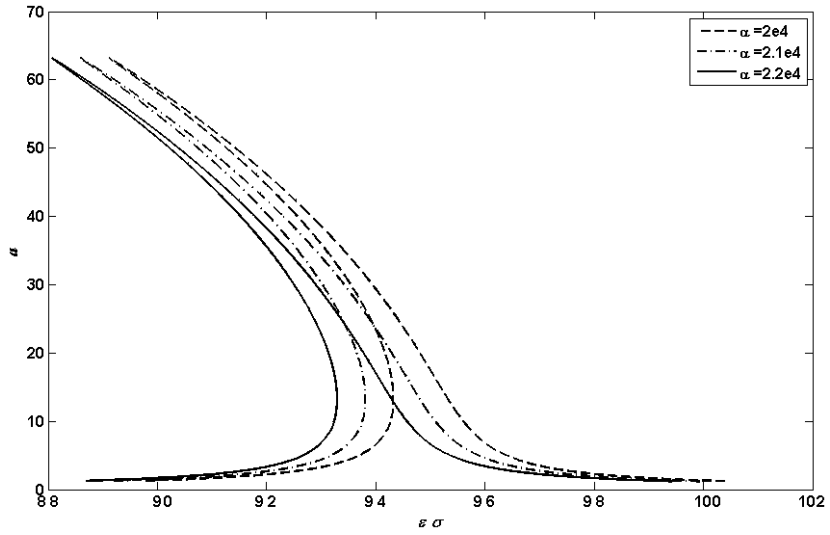

Fig. 7: Effects of a) linear stiffness coefficient of the rail foundation, b) nonlinear stiffness coefficient of the rail foundation, c) damping coefficient of the rail foundation, d) suspension stiffness coefficient of the moving mass, e) suspension damping coefficient of the moving mass, f) rail roughness on the FR of the rail vibration for $\boldsymbol{v + \Omega \approx {\omega_1}/{3}}$

(b)

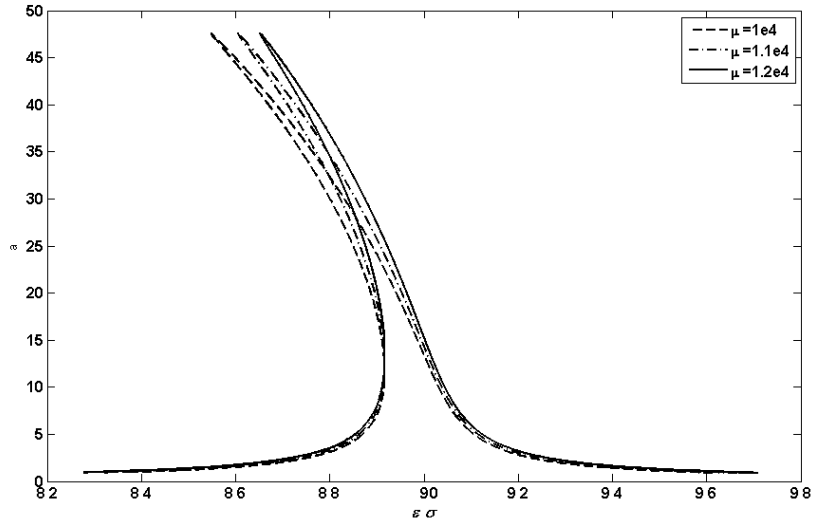

(c)

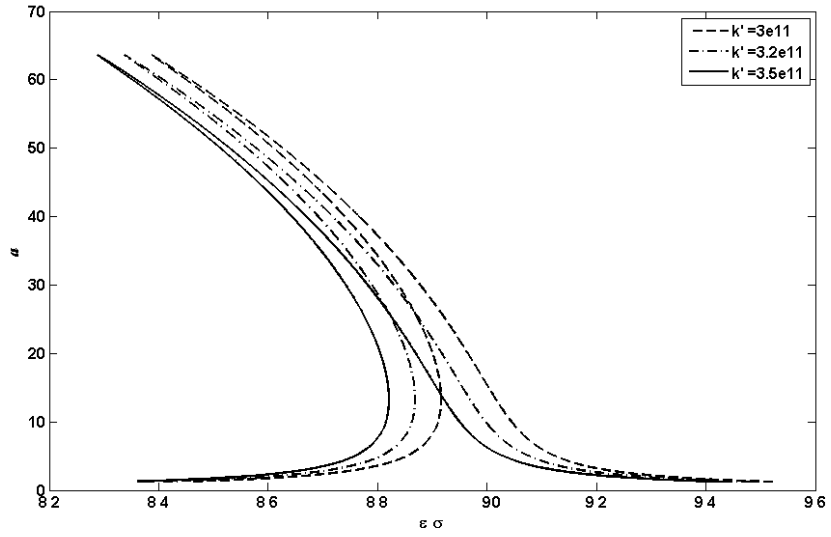

(d)

Fig. 7 (Cont.): Effects of a) linear stiffness coefficient of the rail foundation, b) nonlinear stiffness coefficient of the rail foundation, c) damping coefficient of the rail foundation, d) suspension stiffness coefficient of the moving mass, e) suspension damping coefficient of the moving mass, f) rail roughness on the FR of the rail vibration for $\boldsymbol{\nu + \Omega \approx \omega_1/3}$

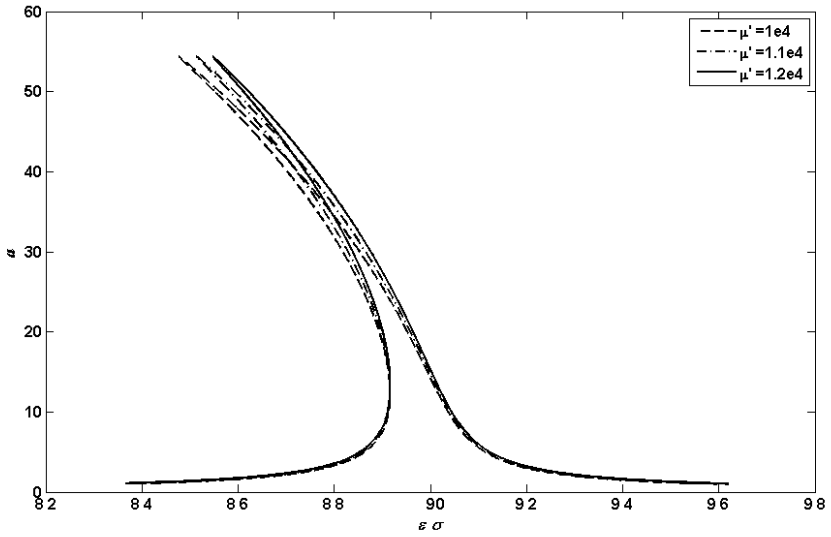

(e)

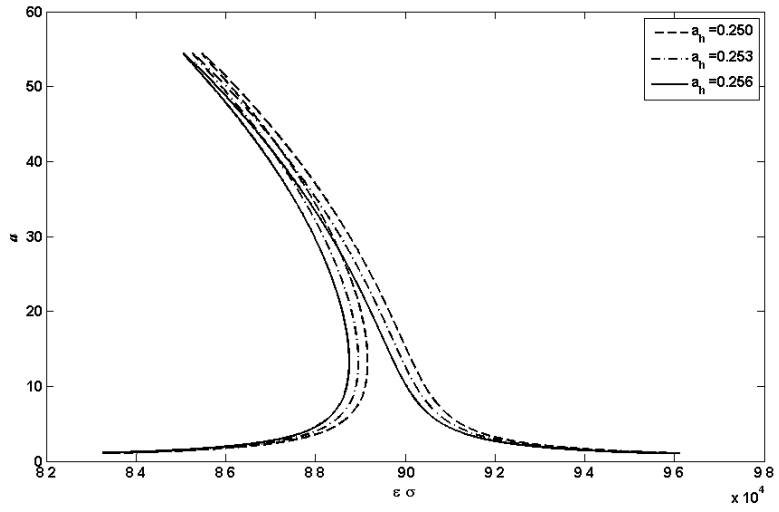

(f)

Fig. 7 (Cont.): Effects of a) linear stiffness coefficient of the rail foundation, b) nonlinear stiffness coefficient of the rail foundation, c) damping coefficient of the rail foundation, d) suspension stiffness coefficient of the moving mass, e) suspension damping coefficient of the moving mass, f) rail roughness on the FR of the rail vibration for $\boldsymbol{v + \Omega \approx {\omega_1}/{3}}$

4.6 Case (f) when $\boldsymbol{v - \Omega \approx {\omega_1}/{3}}$

In this section, the frequency responses of the system in terms of the linear and nonlinear stiffness coefficients of the rail foundation, damping coefficient of the rail foundation, stiffness and damping coefficients of the suspension of the moving mass, and rail roughness are examined, and

shown in Figure 8. Similar trends as those achieved for the previous superharmonic resonance case are observed.

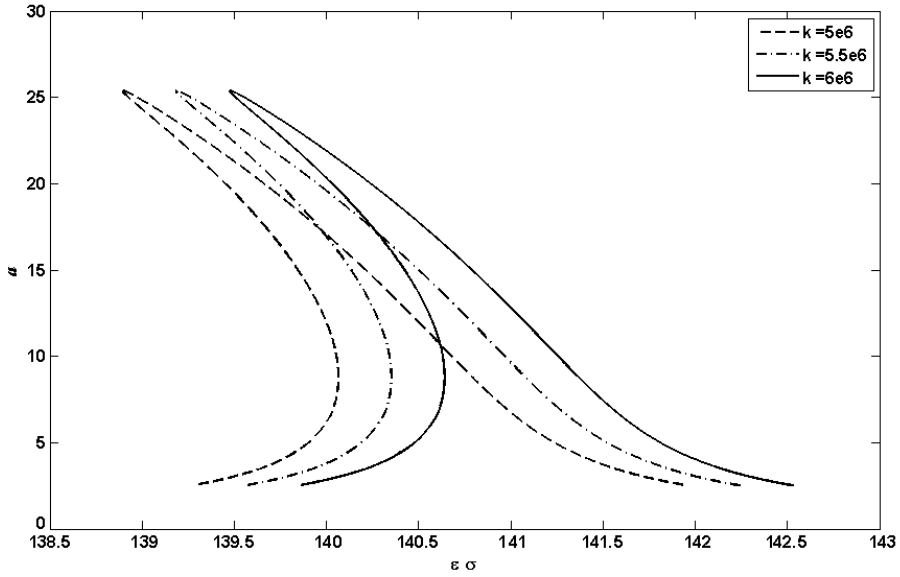

(a)

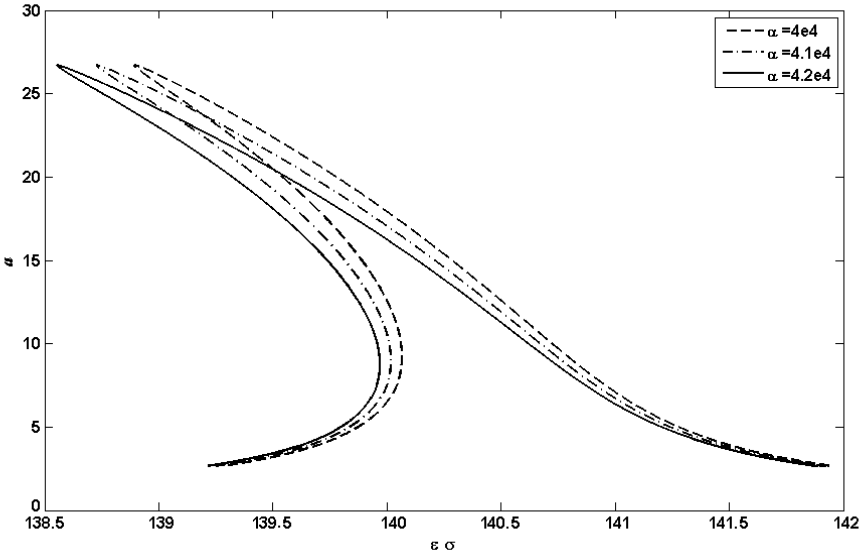

(b)

Fig. 8: Effects of a) linear stiffness coefficient of the rail foundation, b) nonlinear stiffness coefficient of the rail foundation, c) damping coefficient of the rail foundation, d) suspension stiffness coefficient of the moving mass, e) suspension damping coefficient of the moving mass, f) rail roughness on the FR of the rail vibration for $\boldsymbol{\nu - \Omega \approx \omega_1/3}$

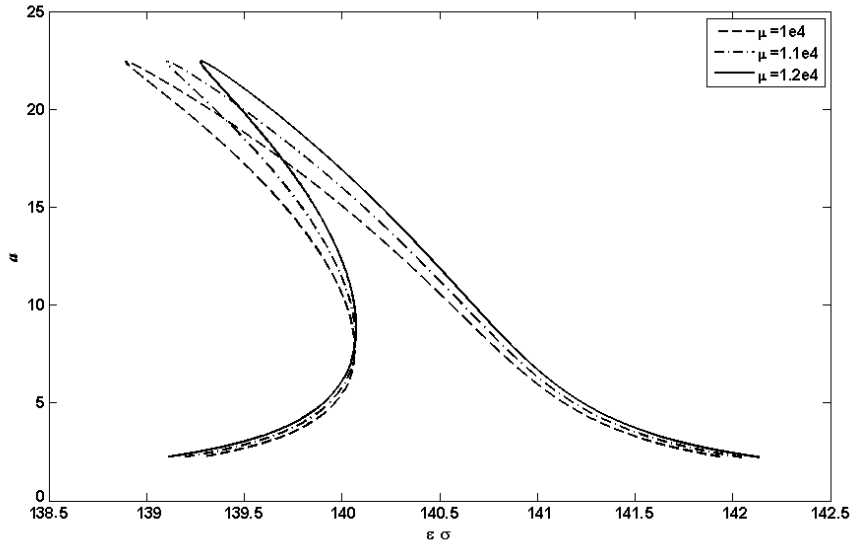

(c)

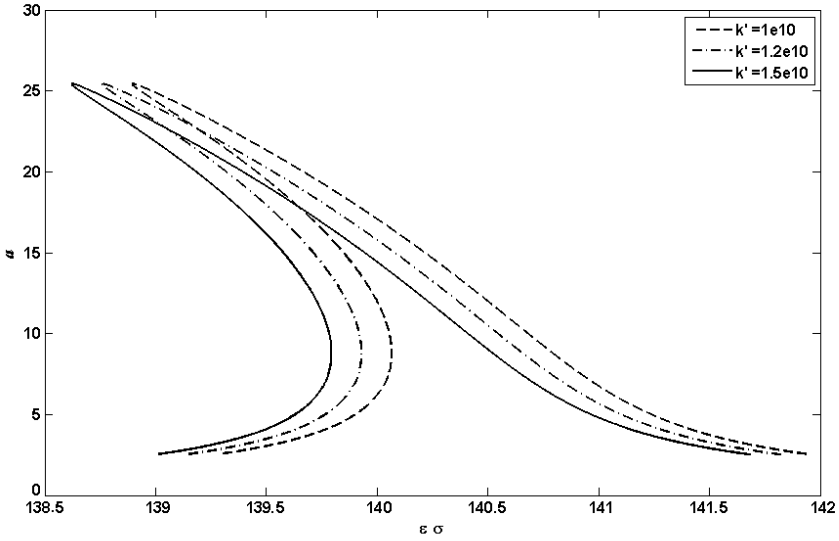

(d)

Fig. 8 (Cont.): Effects of a) linear stiffness coefficient of the rail foundation, b) nonlinear stiffness coefficient of the rail foundation, c) damping coefficient of the rail foundation, d) suspension stiffness coefficient of the moving mass, e) suspension damping coefficient of the moving mass, f) rail roughness on the FR of the rail vibration for $\boldsymbol{v - \Omega \approx \omega_1/3}$

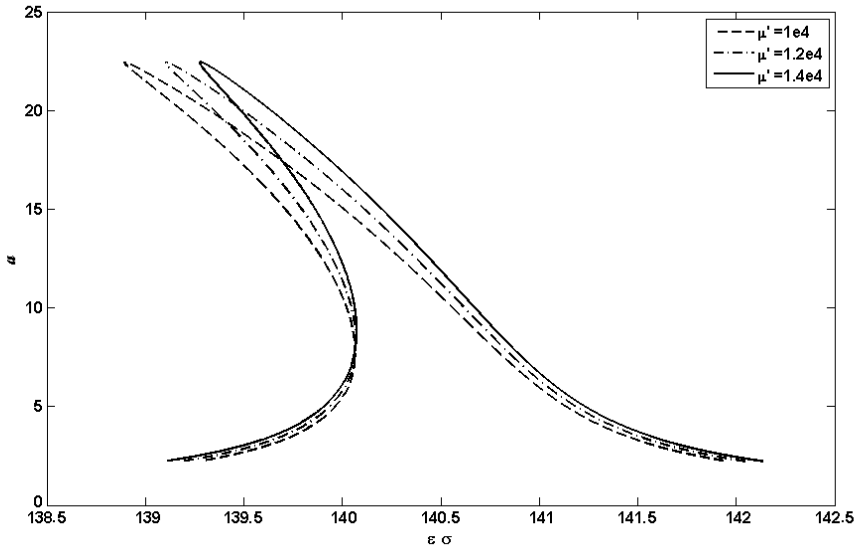

(e)

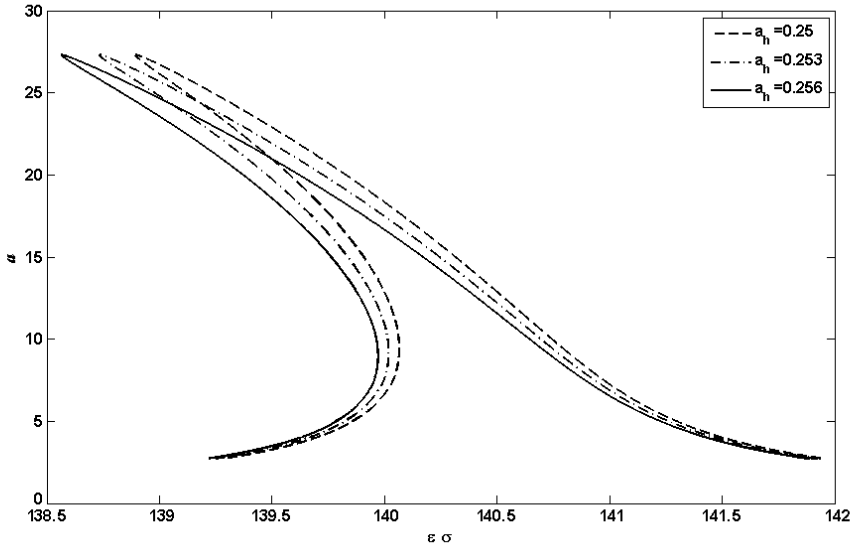

(f)

Fig. 8 (Cont.): Effects of a) linear stiffness coefficient of the rail foundation, b) nonlinear stiffness coefficient of the rail foundation, c) damping coefficient of the rail foundation, d) suspension stiffness coefficient of the moving mass, e) suspension damping coefficient of the moving mass, f) rail roughness on the FR of the rail vibration for $\boldsymbol{v - \Omega \approx \omega_1/3}$

5. Conclusion

This paper analytically investigated the vibration of a beam supported by a nonlinear viscoelastic foundation due to a traveling mass. The Galerkin method was used to derive the coupled nonlinear ordinary differential equations of the system. Additionally, the Multiple Scales method was employed to solve the nonlinear equations of motion. The influences of different parameters, such as characteristics of moving mass suspension, damping coefficient, and nonlinearity of the foundation and the rail roughness on the FR of the system, were studied. The steady-state responses of the primary harmonic as well as its sub and super harmonics, were analytically obtained. The results show that the jump phenomenon would occur only in the FR of the superharmonics. For each of the two superharmonic resonance cases, the jump frequencies would decrease with the decrease of the magnitudes of the linear stiffness of the rail foundation. Therefore, this parameter plays a positive role in the design of railway tracks because of the delay in the jump phenomenon. All parameters investigated do not affect the peak values of the FR; hence, the backbone curve is not observed.

Declaration of competing interest

The authors declare that they have no competing financial interests or personal relationships that could have appeared to influence the work reported in this paper.

Appendix

The results of inserting the solutions of Eqs. (30) and (31) into Eq. (29).

$$D_0^2 u_1 + \omega_1^2 u_1 = -2A'\omega_1 e^{i\omega_1 T_0} - \hat{\mu}_c\left(i\omega_1 A e^{i\omega_1 T_0} + iP(v-\Omega)e^{i(v-\Omega)T_0} - iQ(v+\Omega)e^{i(v+\Omega)T_0}\right)$$
$$-\hat{\alpha}_c\,[A^3 e^{3i\omega_1 T_0} + P^3 e^{3i(v-\Omega)T_0} - Q^3 e^{3i(v+\Omega)T_0} + 3Ae^{i\omega_1 T_0}\left(P^2 e^{2i(v-\Omega)T_0} + Q^2 e^{2i(v+\Omega)T_0}\right)$$
$$+3\bar{A}e^{-i\omega_1 T_0}\left(A^2 e^{2i\omega_1 T_0} + P^2 e^{2i(v-\Omega)T_0} + Q^2 e^{2i(v+\Omega)T_0}\right) + 3Pe^{i(v-\Omega)T_0}\left(A^2 e^{2i\omega_1 T_0} + Q^2 e^{2i(v+\Omega)T_0}\right)$$
$$+3Pe^{-i(v-\Omega)T_0}\left(A^2 e^{2i\omega_1 T_0} + P^2 e^{2i(v-\Omega)T_0} + Q^2 e^{2i(v+\Omega)T_0}\right) + 3Qe^{i(v+\Omega)T_0}\left(A^2 e^{2i\omega_1 T_0} + P^2 e^{2i(v-\Omega)T_0}\right)$$
$$+3Qe^{-i(v+\Omega)T_0}\left(A^2 e^{2i\omega_1 T_0} + P^2 e^{2i(v-\Omega)T_0} + Q^2 e^{2i(v+\Omega)T_0}\right) + 6A\bar{A}\left(Pe^{i(v-\Omega)T_0} - Qe^{i(v+\Omega)T_0}\right)$$
$$+6APe^{i(v-\Omega+\omega_1)T_0}\left(Pe^{-i(v-\Omega)T_0} - Qe^{i(v+\Omega)T_0} - Qe^{-i(v+\Omega)T_0}\right) + 6APe^{-i(v-\Omega-\omega_1)T_0}\left(-Qe^{i(v+\Omega)T_0} -\right.$$
$$\left.Qe^{-i(v+\Omega)T_0}\right) + 6AQ^2 e^{i\omega_1 T_0} + 6P^2\left(-Qe^{i(v+\Omega)T_0}\right) + 6PQ^2 e^{i(v-\Omega)T_0}] + \hat{k}_c'\,[\frac{B}{2i}\left(e^{i(\omega_2+\Omega)T_0} -\right.$$
$$\left.e^{i(\omega_2-\Omega)T_0}\right) + \frac{\omega_2^2}{4}(\lambda_1 e^{i(\omega_1-2\Omega)T_0} + \lambda_1 e^{i\omega_1 T_0} +$$
$$\lambda_2 e^{i(\omega_1-2\Omega)T_0} - \lambda_2 e^{i\omega_1 T_0} + \lambda_3 e^{i(v+\Omega)T_0} - \lambda_3 e^{i(v-\Omega)T_0} + \lambda_4 e^{i(3\Omega-v)T_0} - \lambda_4 e^{i(\Omega-v)T_0} - \lambda_5 e^{i(3\Omega+v)T_0} + \lambda_5 e^{i(\Omega+\iota}$$
$$-\lambda_7 e^{i(\Omega+v)T_0} + \lambda_7 e^{i(v-\Omega)T_0})] + \frac{\hat{k}_c'}{4}\,[A\left(e^{i(\omega_1+2\Omega)T_0} + e^{i(\omega_1-2\Omega)T_0} - 2e^{i\omega_1 T_0}\right) + (Pe^{i(v+\Omega)T_0}$$
$$+Pe^{-i(v-3\Omega)T_0} + Qe^{i(v+3\Omega)T_0} + Qe^{i(\Omega-v)T_0} - 2Pe^{i(v-\Omega)T_0} + 2Qe^{i(v+\Omega)T_0})] + \hat{\mu}'_c[i\omega_2 B e^{i\omega_2 T_0} +$$
$$\frac{\omega_2^2}{2}(\lambda_1(\omega_1+\Omega)e^{i(\omega_1+\Omega)T_0} - \lambda_2(\omega_1-\Omega)e^{i(\omega_1-\Omega)T_0} + \lambda_3 v e^{ivT_0} + \lambda_4(2\Omega-v)e^{i(2\Omega-v)T_0}$$
$$-\lambda_5(v+2\Omega)e^{i(\omega_1+2\Omega)T_0} + \lambda_6 v e^{ivT_0} + \lambda_7 v e^{ivT_0}) - \frac{1}{4i}(\omega_1 A e^{i(\omega_1+2\Omega)T_0} + P(v-\Omega)e^{i(v+\Omega)T_0} -$$
$$Q(v+\Omega)e^{i(v+3\Omega)T_0}\,2\omega_1 A e^{i\omega_1 T_0} + 2P(v-\Omega)e^{i(v-\Omega)T_0} - 2Q(v+\Omega)e^{i(v+\Omega)T_0}\,\omega_1 A e^{i(\omega_1-2\Omega)T_0} +$$
$$P(v-\Omega)e^{i(v-3\Omega)T_0} - Q(v+\Omega)e^{i(v+\Omega)T_0}) - \frac{\hat{a}v}{4i}(e^{i(v+\Omega)T_0} + e^{i(\Omega-v)T_0})] + cc \qquad \text{(A-1)}$$

$$D_0^2 y_1 + \omega_2^2 y_1 = -2\omega_2 i\acute{B}e^{i\omega_2 T_0} - \acute{\mu_c}\omega_2 i\acute{B}e^{i\omega_2 T_0} - \hat{g} - \frac{\omega_2^2}{2i}(e^{i\Omega T_0} - e^{-i\Omega T_0}) \qquad [+Ce^{i\omega_1 T_0} -$$
$$\mu_0\left[\frac{P_i(v-\Omega)}{\omega_1^2-(v-\Omega)^2}e^{i(v-\Omega)T_0} - \frac{Q_i(v-\Omega)}{\omega_1^2-(v-\Omega)^2}e^{i(v-\Omega)T_0}\right] + \hat{\alpha}_c[\frac{A^3}{-8\omega_1^2}e^{3i\omega_1 T_0} + \frac{P^3}{\omega_1^2-9(v-\Omega)^3}e^{3i(v-\Omega)T_0}$$
$$-\frac{Q^3}{\omega_1^2-9(v-\Omega)^2}e^{3i(v-\Omega)T_0} + \frac{3AP^3}{\omega_1^2-\left(\omega_1^2+2v-2\Omega\right)^3}e^{i(\omega_1+2v-2\Omega)T_0} + \frac{3AQ^3}{\omega_1^2-\left(\omega_1^2+2v+2\Omega\right)^2}e^{i(\omega_1-2v-2\Omega)T_0}$$
$$+\frac{3\underline{A}P^3}{\omega_1^2-(2v-2\Omega-\omega_1)^2}e^{i(2v-2\Omega-\omega_1)T_0} + \frac{3\underline{A}Q^3}{\omega_1^2-(2v+2\Omega-\omega_1)^2}e^{i(2v-2\Omega-\omega_1)T_0} + \frac{3PA^2}{\omega_1^2-(v-\Omega-2\omega_1)^2}e^{i(v-\Omega-2\omega_1)T_0} \qquad \text{(A-2)}$$
$$+\frac{3PQ^2}{\omega_1^2-(3v+\Omega)^2}e^{i(3v+\Omega)T_0} + \frac{3PA^2}{\omega_1^2-(\Omega+2\omega_1-v)^2}e^{i(\Omega+2\omega_1-v)T_0} + \frac{3P^3}{\omega_1^2-(v-\Omega)^2}e^{i(v-\Omega)T_0} + \frac{3PQ^2}{\omega_1^2-(3v+\Omega)^2}e^{i(3v+\Omega)T_0}$$
$$+\frac{3QA^2}{\omega_1^2-(v+\Omega+2\omega_1)^2}e^{i(v+\Omega+2\omega_1)T_0} + \frac{3\alpha P^2}{\omega_1^2-(3v-\Omega)^2}e^{i(3v-\Omega)T_0} + \frac{3QA^2}{\omega_1^2-(2\omega_1-v-\Omega)^2}e^{i(2\omega_1-v-\Omega)T_0}$$

$$+\frac{3\alpha P^2}{\omega_1^2-(3v-\Omega)^2}e^{i(3v-\Omega)T_0}+\frac{3QA^2}{\omega_1^2-(2\omega_1-v-\Omega)^2}e^{i(2\omega_1-v-\Omega)T_0}+\frac{3QP^2}{\omega_1^2-(v-3\Omega)^2}e^{i(v-3\Omega)T_0}+\frac{3Q^3}{\omega_1^2-(v+\Omega)^2}e^{i(v+\Omega)T_0}$$

$$+\frac{6A\underline{A}P}{\omega_1^2-(v-\Omega)^2}e^{i(v-\Omega)T_0}-\frac{6A\underline{A}P}{\omega_1^2-(v+\Omega)^2}e^{i(v+\Omega)T_0}-\frac{6AQP}{\omega_1^2-(2v+\omega_1)^2}e^{i(2v+\omega_1)T_0}-\frac{6APQ}{\omega_1^2-(2\Omega+\omega_1)^2}e^{i(2\Omega+\omega_1)T_0}$$

$$-\frac{6P^2Q}{\omega_1^2-(v+\Omega)^2}e^{i(v+\Omega)T_0}+\frac{6PQ^2}{\omega_1^2-(v-\Omega)^2}e^{i(v-\Omega)T_0}]+\hat{k}_c[\frac{B}{2i(\omega_1^2-(\omega_2+\Omega)^2)}e^{i(\omega_2+\Omega)T_0}-$$

$$\frac{B}{2i(\omega_1^2-(\omega_2-\Omega)^2)}e^{i(\omega_2-\Omega)T_0}$$

$$+\frac{\omega_1^4}{4}\left(\frac{\lambda_1}{(\omega_1^2-(\omega_1+2\Omega)^2)}e^{i(\omega_1+2\Omega)T_0}+\frac{\lambda_2}{(\omega_1^2-(\omega_1-2\Omega)^2)}e^{i(\omega_1-2\Omega)T_0}\right)+\frac{\lambda_3}{(\omega_1^2-(v+\Omega)^2)}e^{i(v+\Omega)T_0}-$$

$$\frac{\lambda_3}{(\omega_1^2-(v-\Omega)^2)}e^{i(v-\Omega)T_0}$$

$$+\frac{\lambda_4}{(\omega_1^2-(3\Omega-v)^2)}e^{i(3\Omega-v)T_0}-\frac{\lambda_4}{(\omega_1^2-(\Omega-v)^2)}e^{i(\Omega-v)T_0}-\frac{\lambda_5}{(\omega_1^2-(v+3\Omega)^2)}e^{i(v+3\Omega)T_0}+\frac{\lambda_5}{(\omega_1^2-(v+\Omega)^2)}e^{i(v+\Omega)T_0}$$

$$+\frac{\lambda_6}{(\omega_1^2-(v+\Omega)^2)}e^{i(v+\Omega)T_0}-\frac{\lambda_6}{(\omega_1^2-(v-\Omega)^2)}e^{i(v-\Omega)T_0}-\frac{\lambda_7}{(\omega_1^2-(v+\Omega)^2)}e^{i(v+\Omega)T_0}+\frac{\lambda_7}{(\omega_1^2-(v-\Omega)^2)}e^{i(v-\Omega)T_0}]$$

$$+\frac{\hat{k}_c}{4}[\frac{A}{\omega_1^2-(\omega_1+2\Omega)^2}e^{i(\omega_1+2\Omega)T_0}+\frac{A}{\omega_1^2-(\omega_1-2\Omega)^2}e^{i(\omega_1-2\Omega)T_0}+\frac{P}{\omega_1^2-(v+\Omega)^2}e^{i(v+\Omega)T_0}+$$

$$\frac{P}{\omega_1^2-(3\Omega-v)^2}e^{i(3\Omega-v)T_0}$$

$$+\frac{Q}{\omega_1^2-(v+3\Omega)^2}e^{i(v+3\Omega)T_0}+\frac{Q}{\omega_1^2-(\Omega-v)^2}e^{i(\Omega-v)T_0}+\frac{2P}{\omega_1^2-(v-\Omega)^2}e^{i(v-\Omega)T_0}+\frac{2Q}{\omega_1^2-(v+\Omega)^2}e^{i(v+\Omega)T_0}]+$$

$$\hat{\mu}'_c[\frac{i\omega_2 B}{\omega_1^2-\omega_2^2}e^{i\omega_2 T_0}+\frac{\omega_2^2}{2}(\frac{\lambda_1(\omega_1+\Omega)}{\omega_1^2-(\omega_1+\Omega)^2}e^{i(\omega_1+\Omega)T_0}-\frac{\lambda_2(\omega_1-\Omega)}{\omega_1^2-(\omega_1-\Omega)^2}e^{i(\omega_1-\Omega)T_0}+\frac{\lambda_3 v}{\omega_1^2-v_2^2}e^{ivT_0}+$$

$$\frac{\lambda_4(2\Omega-v)}{\omega_1^2-(2\Omega-v)^2}e^{i(2\Omega-v)T_0}$$

$$-\frac{\lambda_5(v+2\Omega)}{\omega_1^2-(v+2\Omega)^2}e^{i(\omega_1+2\Omega)T_0}+\frac{\lambda_6 v}{\omega_1^2-v_2^2}e^{ivT_0}+\frac{\lambda_7 v}{\omega_1^2-v_2^2}e^{ivT_0})-\frac{1}{4i}(\frac{\omega_1 A}{\omega_1^2-(\omega_1+2\Omega)^2}e^{i(\omega_1+2\Omega)T_0}+$$

$$\frac{P(v-\Omega)}{\omega_1^2-(v+\Omega)^2}e^{i(v+\Omega)T_0}-\frac{Q(v+\Omega)}{\omega_1^2-(v+3\Omega)^2}e^{i(v+3\Omega)T_0}+\frac{2P(v-\Omega)}{\omega_1^2-(v-\Omega)^2}e^{i(v-\Omega)T_0}-\frac{2Q(v+\Omega)}{\omega_1^2-(v+\Omega)^2}e^{i(v+\Omega)T_0}$$

$$\frac{\omega_1 A}{\omega_1^2-(\omega_1-2\Omega)^2}e^{i(\omega_1-2\Omega)T_0}+\frac{P(v-\Omega)}{\omega_1^2-(v-3\Omega)^2}e^{i(v-3\Omega)T_0}-\frac{Q(v+\Omega)}{\omega_1^2-(v-3\Omega)^2}e^{i(v+\Omega)T_0})-\frac{\hat{a}v}{4i}(\frac{e^{i(v+\Omega)T_0}}{\omega_1^2-(\omega_1+\Omega)^2}+$$

$$\frac{e^{i(\Omega-v)T_0}}{\omega_1^2-(\Omega-v)^2})]]+cc$$

where $\lambda_1=\frac{A}{(\omega_2^2-(\omega_1+\Omega)^2)}$, $\lambda_2=\frac{A}{(\omega_2^2-(\omega_1-\Omega)^2)}$, $\lambda_3=\frac{P}{(\omega_2^2-v^2)}$, $\lambda_4=\frac{P}{(\omega_2^2-(2\Omega-v)^2)}$, $\lambda_5=\frac{Q}{(\omega_2^2-(v+2\Omega)^2)}$, $\lambda_6=\frac{Q}{(\omega_2^2-v^2)}$ and $\lambda_7=\frac{a}{(\omega_2^2-v^2)}$.

References

[1] R. Dong, S. Sankar, R. Dukkipati, A finite element model of railway track and its application to the wheel flat problem, Proceedings of the Institution of Mechanical Engineers, Part F: Journal of Rail and Rapid Transit, 208 (1994) 61-72.
[2] M.R. Pfaffinger, J. Dual, Higher vibration modes in railway tracks at their cut-off frequencies, Journal of sound and vibration, 253 (2002) 1015-1037.
[3] E. Çelebi, Three-dimensional modelling of train-track and sub-soil analysis for surface vibrations due to moving loads, Applied Mathematics and Computation, 179 (2006) 209-230.
[4] Z. Dimitrovová, J. Varandas, Critical velocity of a load moving on a beam with a sudden change of foundation stiffness: Applications to high-speed trains, Computers & Structures, 87 (2009) 1224-1232.
[5] D. Zheng, S. Fan, Instability of vibration of a moving-train-and-rail coupling system, Journal of sound and vibration, 255 (2002) 243-259.
[6] W. Zhai, X. Sun, A detailed model for investigating vertical interaction between railway vehicle and track, vehicle system dynamics, 23 (1994) 603-615.
[7] Y.Q. Sun, M. Dhanasekar, A dynamic model for the vertical interaction of the rail track and wagon system, International journal of solids and structures, 39 (2002) 1337-1359.
[8] I. Coskun, H. Engin, Non-linear vibrations of a beam on an elastic foundation, Journal of Sound and Vibration, 223 (1999) 335-354.
[9] M. Ansari, E. Esmailzadeh, D. Younesian, Internal-external resonance of beams on non-linear viscoelastic foundation traversed by moving load, Nonlinear Dynamics, 61 (2010) 163-182.
[10] M. Ansari, E. Esmailzadeh, D. Younesian, Frequency analysis of finite beams on nonlinear Kelvin–Voight foundation under moving loads, Journal of Sound and Vibration, 330 (2011) 1455-1471.
[11] A.Y. Wayou, R. Tchoukuegno, P. Woafo, Non-linear dynamics of an elastic beam under moving loads, Journal of Sound and Vibration, 273 (2004) 1101-1108.
[12] B. Kang, C. Tan, Nonlinear response of a beam under distributed moving contact load, Communications in Nonlinear Science and Numerical Simulation, 11 (2006) 203-232.
[13] D.M. Santee, P.B. Gonçalves, Oscillations of a Beam on a Non-Linear Elastic Foundation under Periodic Loads, Shock and Vibration, 13 (2006) 273-284.
[14] D. Froio, E. Rizzi, F.M. Simões, A.P. da Costa, Critical velocities of a beam on nonlinear elastic foundation under harmonic moving load, Procedia engineering, 199 (2017) 2585-2590.
[15] B. Zhen, J. Xu, J. Sun, Analytical solutions for steady state responses of an infinite Euler-Bernoulli beam on a nonlinear viscoelastic foundation subjected to a harmonic moving load, Journal of Sound and Vibration, 476 (2020) 115271.
[16] R.N. Jazar, Advanced Vibrations: Theory and Application, Springer Nature, 2023.
[17] A.H. Nayfeh, D.T. Mook, Nonlinear oscillations, John Wiley & Sons, 2008.
[18] H. Wei, Z. Yida, The dynamic response of a viscoelastic Winkler foundation-supported elastic beam impacted by a low velocity projectile, Computers & structures, 52 (1994) 431-436.